Research Article

Hao Liu, Chan Wang*, Yong Li, Jianghong Deng, Bin Deng, Yuexing Feng, Hui Chen, Yunlong Xu, and Shaoze Zhao

Geochemistry of the black rock series of lower Cambrian Qiongzhusi Formation, SW Yangtze Block, China: Reconstruction of sedimentary and tectonic environments

https://doi.org/10.1515/geo-2020-0228
received August 05, 2020; accepted January 24, 2021

Abstract: The black rock series in the Qiongzhusi Formation contains important geochemical information about the early Cambrian tectonic and ecological environment of the southwestern Yangtze Block. In this paper, major, trace, and rare earth element data are presented in an attempt to reveal the sediment source during the deposition of the early Cambrian Qiongzhusi Formation and to reconstruct the sedimentary tectonic environment and weathering intensity during that time. The basin primarily received continental clastic material with neutral-acidic igneous rocks from a stable source and with a moderate level of maturity during the depositional period of the Qiongzhusi Formation. Furthermore, the strata were weakly influenced by submarine hydrothermal fluids during diagenesis. The reconstruction of the sedimentary environment and weathering intensity shows that P_2O_5 enrichment and water body stratification occurred due to the effects of upwelling ocean currents during the depositional period of the Qiongzhusi Formation. The combination of upwelling and bottom-water hydrothermal fluids led to environmental changes in the study area, from dry and hot to moist and warm. Last, the reconstruction of the tectonic environment of the Qiongzhusi Formation indicates that deposition occurred in continental slope and marginal marine environments associated with a continental arc tectonic system. These findings provide an essential basis for the comprehensive reconstruction of the early Cambrian sedimentary environment of the Yangtze Block.

Keywords: geochemistry, black rock series, Cambrian, depositional environment, Yangtze Block, South China

1 Introduction

The early Cambrian was a very important period of geological history [1–4] because Ediacaran fauna disappeared at the end of the Neoproterozoic and an important biological diversification event called the Cambrian explosion occurred during this epoch, during which skeletal animals emerged [4–7]. This diversification event produced considerable organic matter, leading to the formation of high-quality oil and gas deposits, and this organic matter was preserved in various sedimentary environments and paleoclimates at that time [7–10]. Therefore, it is of great geological interest to study the sedimentary and climatic environment of black rock series with oil- and gas-rich beds.

In southwestern China, the Yangtze Block has large amounts of preserved sedimentary rocks that formed over several periods in different environments [8–10]. The widespread lower Cambrian black rock series in the Upper Yangtze region was deposited in a shallow-shelf setting and thus provides a very important window for documenting the early Cambrian sedimentary-tectonic-ecological environment of South China [8,11–14]. However, some key issues regarding the early Cambrian marine sedimentary environment along the southwestern margin of the Yangtze Block still remain unclear; for example, how was hot, phosphorus-rich water released from the seafloor along the southwestern margin of the early Cambrian Yangtze Block? How did this release affect the enrichment of elements? How did the upwelling current affect the environment?

* **Corresponding author: Chan Wang,** Key Laboratory of Ocean and Marginal Sea Geology, South China Sea Institute of Oceanology, Innovation Academy of South China Sea Ecology and Environmental Engineering, Chinese Academy of Sciences, Guangzhou 510301, China; Southern Marine Science and Engineering Guangdong Laboratory (Guangzhou), Guangzhou 511458, China, e-mail: 271980531@qq.com
Hao Liu, Yunlong Xu, Shaoze Zhao: College of Energy, Chengdu University of Technology, Chengdu 610059, China
Yong Li: College of Geophysics, Chengdu University of Technology, Chengdu 610059, China
Jianghong Deng, Bin Deng, Hui Chen: College of Earth Science, Chengdu University of Technology, Chengdu 610059, China
Yuexing Feng: School of Environment and Earth Science, the University of Queensland, Brisbane 4072, Australia

In this paper, we present a systematic analysis on the geochemistry of the black rock series in the lower Cambrian Qiongzhusi Formation to understand the constraints on the provenance of sedimentary rocks and the sedimentary, ecological, and tectonic environment. Our studies provide basic data for understanding the sedimentary and tectonic evolution along the southwestern margin of the Yangtze Block during the early Cambrian, and thus they provide an essential basis for the comprehensive reconstruction of the early Cambrian sedimentary and tectonic environment of the Yangtze Block.

2 Geologic setting

The Yangtze Block in eastern China is separated from the North China Craton to the north by the Qinling–Dabie orogen, from the Cathaysia block to the southeast by the Jiangnan orogen, and from the Songpan–Ganzi complex to the west by the Longmenshan fault zone [15,16] (Figure 1a). It is generally believed that the Yangtze Block is underlain by an Archean cratonic basement and that the block collided with the Cathaysia block during the Neoproterozoic, together forming part of the Rodinia supercontinent [17]. Throughout the Paleozoic, the Yangtze Block was a stable passive continental margin that was subject to extensive platform-style marine sedimentation (Figure 1b).

The research area is located in the eastern segment of the Meigu-Jinyang depression in the western Yangtze Block (approximately the Sichuan basin) (Figure 1b). The black rock series of the Qiongzhusi Formation is widespread in the Sichuan basin and constitutes a set of hypoxic deposits with an extremely subtle phase transition [19–21]. The seawater depth on the passive continental margin of the Paleo-Tethys Ocean increased rapidly from southeast to northwest, which led to a gradual increase in the continental shelf area, resulting in a degree of deepening of the seawater and an increase in the extent of eroded bedrock surface. As a result of a transgression, a zone in which photosynthesis could occur arose, which led to a gradual decrease in the photosynthesis in the lower part of the water column and a continuous increase in oxygen consumption in the water [22,23]. Therefore, rising sea levels led to an increased oxygen-deficient environment in the lower part of the water column. In addition, the rising sea level entrained terrestrial plant debris, transported this terrestrial plant material out to sea, increased the amount of available organic matter, and led to the flourishing of large amounts of plankton, which increased the organic matter contents in the sediments [33]. Nutrients were brought to the surface, biological productivity was high, and oxygen consumption increased because of the influence of upwelling oceanic currents in the continental slope zone. These processes resulted in the formation of a reductive sedimentary environment and the formation of the early Cambrian black rock series in the study area [37].

The paleogeographic environment of the study area featured the following settings from NW to SE: shore,

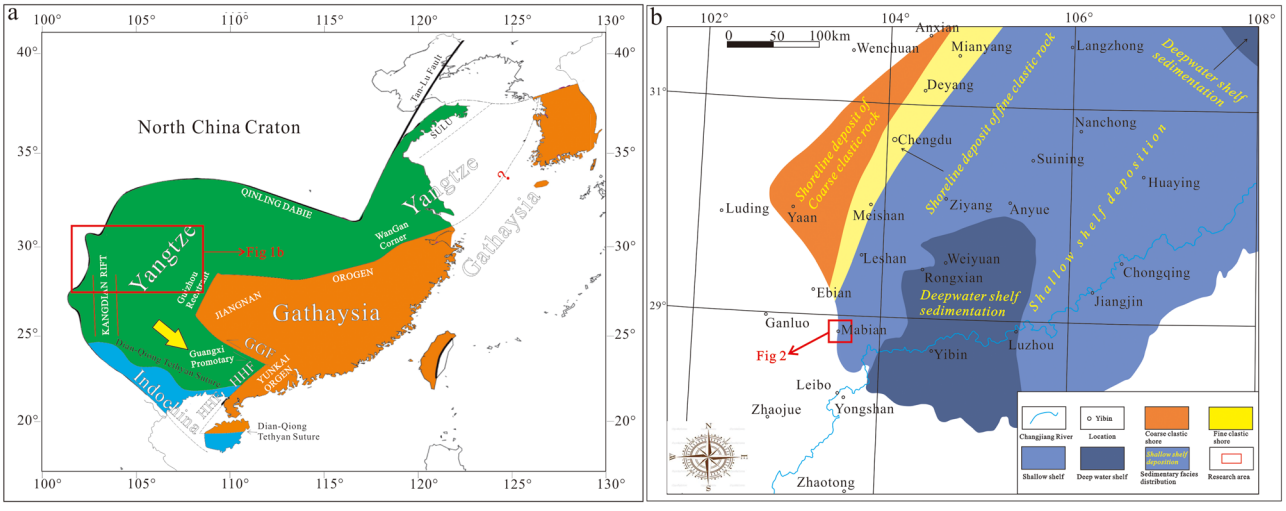

Figure 1: Distributions of the Precambrian basement and tectonic divisions of South China. The boundary between South China and Indochina follows [17]. GGF-Guangzhou-Guiyang basement fault; HHF-Hetai-Hepu fault (a); the lithofacies paleogeography of the Cambrian Qiongzhusi Formation in the Sichuan basin (b) (Figure 1b modified after [18]).

inner shelf, outer shelf, and shelf margin and deep-water basin [24,25]. Source rocks with extremely stable distributions developed in the facies of the shelf and shelf margin, representing the second set of regional source rocks with good hydrocarbon generation ability in the region [26]. All these characteristics show that the southwestern Sichuan basin was completely inundated by the sea during the early Cambrian. The study area was located in a semi-restricted and semi-open deep-water shelf setting and was connected to the western Hubei deep-water shelf to the east [27]. Therefore, the sedimentary facies of the Upper Yangtze region in the early Cambrian from west to east were the Kangdian ancient land, shore, shallow shelf, southern Sichuan deep-water shelf, shallow-water shelf (Dingshan underwater highland), eastern Sichuan-western Hubei deep-water shelf, slope, and deep-water basin. The southern Sichuan basin was located on the eastern, western, and northern sides of the shallow-water shelf surrounding a deep-water environment (the ancient South China Ocean) with poor connectivity to the outer sea (Figure 2).

The lithology is characterized by a set of littoral to shallow-facies clastic rocks and carbonate deposits that represent the cyclic characteristics of a marine advance, regression, and advance. The Cambrian strata can be divided into the lower Maidiping Formation, Qiongzhusi Formation, Canglangpu Formation, Longwangmiao Formation, middle Douposi Formation, and middle-upper Edaoshui Formation [28–30]. The Cambrian strata cover the Sinian Dengying Formation in a disconformable contact and are the overlying Ordovician Hongshiya Formation (Figure 3), and the contact with the overlying Canglangpu Formation of the Cambrian system is conformable in the measured section in the research area. The beginning of the Cambrian is characterized by dolomite to fine sandstone, and the primary lithologies are calcareous and dolomitic siltstone, dolomitic fine sandstone, and mudstone. The lithofacies of the Cambrian Qiongzhusi Formation

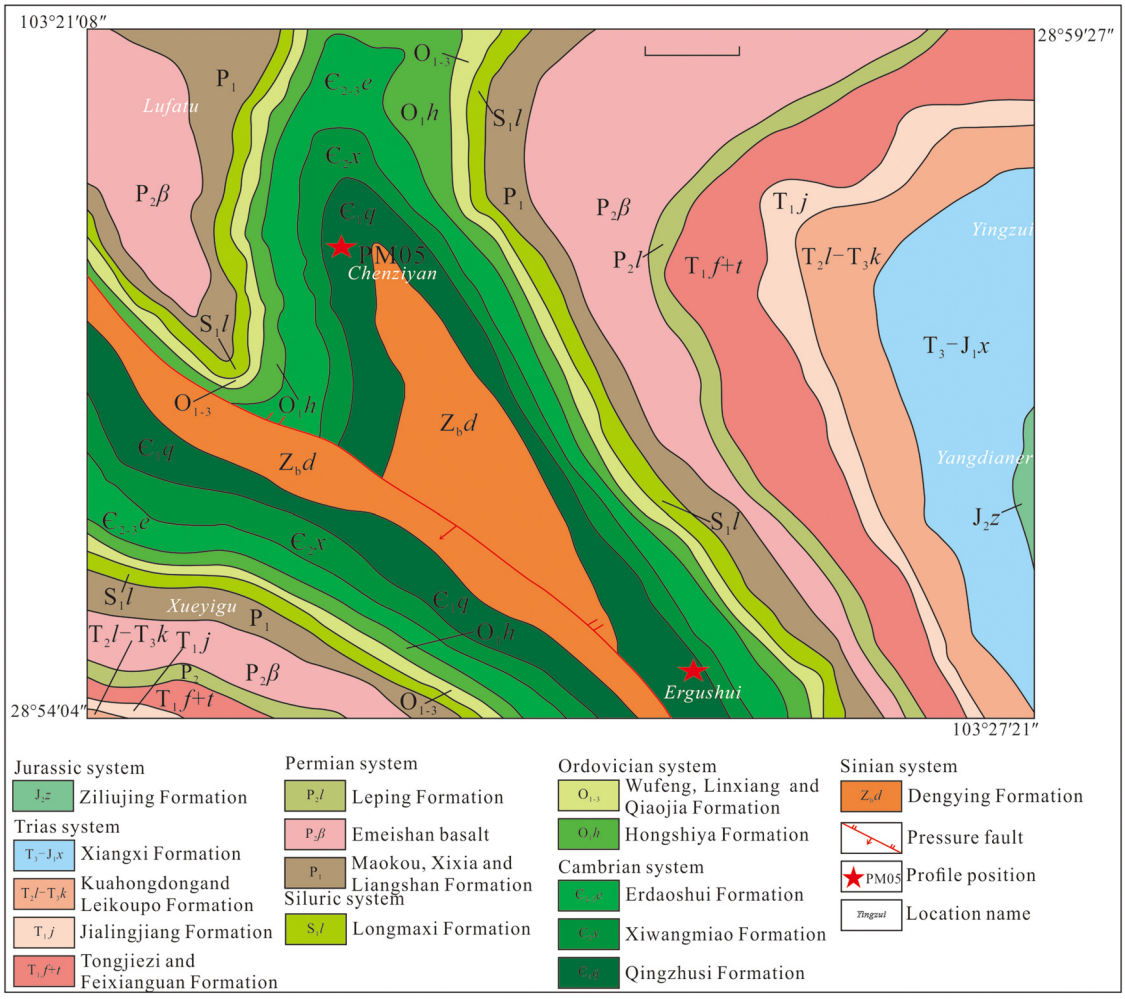

Figure 2: Geological structure map showing the location of the section.

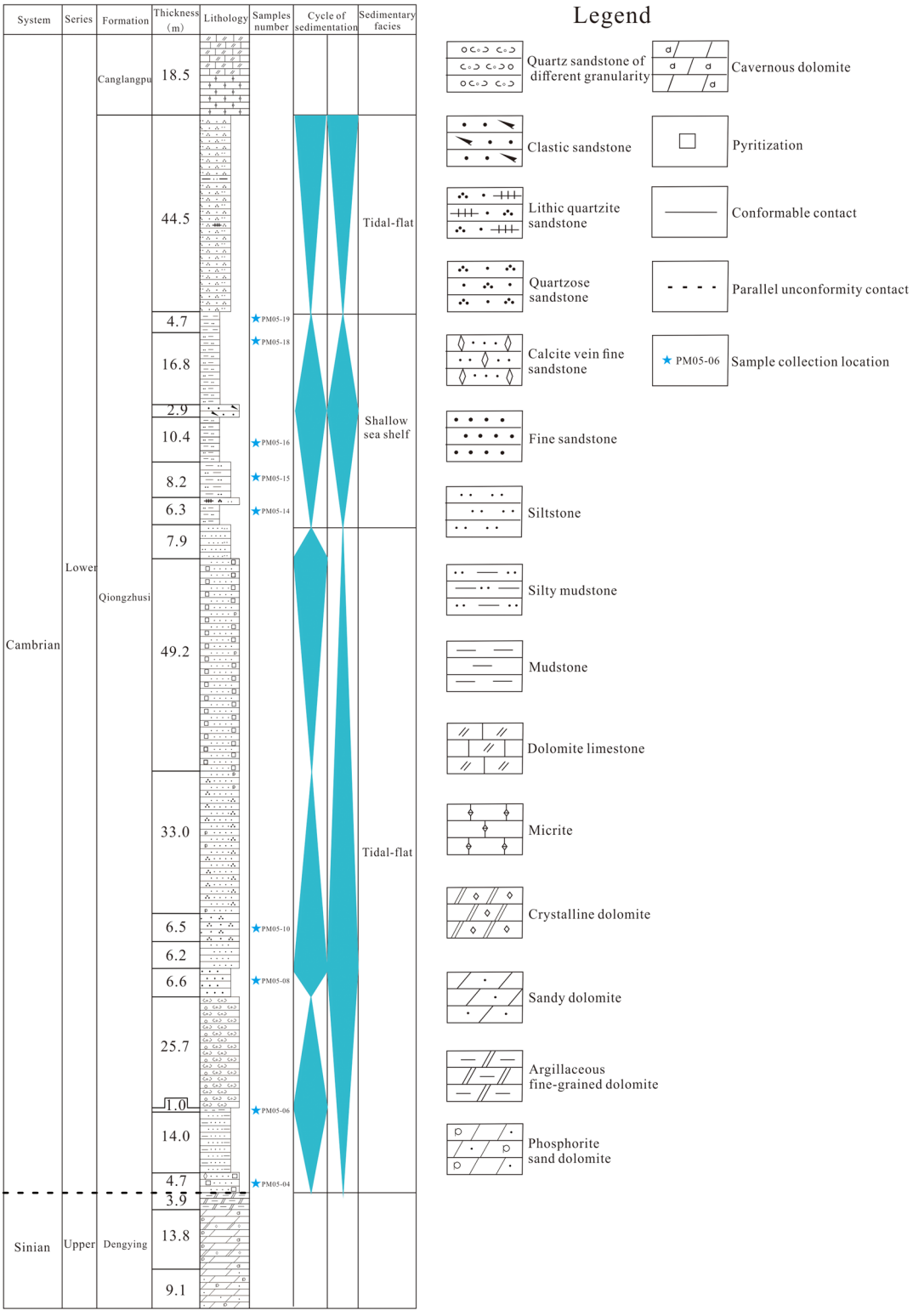

Figure 3: Stratigraphic, lithologic, and structural setting of the Qiongzhusi Formation in the Mabian area.

alternate between the littoral facies and the shallow-sea facies. The early and late periods were tidal flat facies environments, and the middle period featured a shallow-sea shelf environment. The above results indicate that the Cambrian Qiongzhusi Formation is dominated by siliciclastic sedimentary rocks and that carbonate material was involved

in the depositional process. Based on the division of sedimentary facies from the bottom to the top, a process of water body deepening and then shallowing occurred.

3 Sampling and analytical methods

Ten samples were collected from throughout the Cambrian Qiongzhusi Formation from a section in the Mabian area along the southwestern margin of the Yangtze Block (Figure 2). Sample D0505 represents the black mudstone in the Cambrian Qiongzhusi Formation which was deposited in the deeper waters of the eastern side (Figure 3), and it was primarily examined for comparison with the section data. None of the collected samples was affected by weathering, alteration, etc. All the samples are black mudstone or sandstone.

A geochemical analysis of all the samples was conducted at the Sichuan Metallurgical Geological Rocks and Minerals Analytic Center, Chengdu, China. All the analysis results were referenced to the DZG20-01 standard, and the analyses were completed using a Thermo Electron Corporation ICAP QC inductively coupled plasma-mass spectrometer (ICP-MS) and Thermo ICAP 6300 inductively coupled plasma-atomic emission spectroscope (ICP-AES) instruments, with volumetric and plasma emission spectrometry being performed at a room temperature of 23°C and a humidity of 62% [30,31].

SiO_2, Al_2O_3, Fe_2O_3, CaO, MgO, K_2O, Na_2O, P_2O_5, TiO_2, MnO, and other major element oxides were analyzed using the same procedure as that reported by Kimura [9] for ICP-AES. The uncertainty of the analysis was usually less than 5%. The trace element contents were measured by ICP-MS. The analytical method is similar to that of Jones et al. [34]. HF + HNO_3 (HF:HNO_3 = 1:2) was used to dissolve the samples in a microwave furnace. The detection limit of the elements was $0.1 - n \times 10^{-12}$ (n = 1–9) [32].

4 Results

4.1 Petrography

The petrographic characteristics indicate that the section comprises a large number of silty to fine sandstones with a small amount of glutenite and that the proportion of sand in the lithology gradually decreases toward the southeast. These characteristics suggest that the sedimentary environment changes from deep-water shelf sediments in the lower part (phosphorous argillaceous siltstone) to shallow-water shelf sediments in the upper part (silty mudstone and lithic quartz sandstone) (Figure 3). Under the microscope, the samples exhibit uneven distributions of dolomite metacrysts, quartz metacrysts, collophanite, iron, and metal minerals in the lower Formation and an uneven distributions of silt and sand in the matrix of the upper Formation. The rocks have undergone post-diagenetic dolomitization. Markers of a reducing environment (collophanite and pyrite) can also be clearly observed in the Qiongzhusi Formation, which indicates that the study area was a large-scale hypoxic environment during the early Cambrian period. In this study, the results of the corresponding organic carbon content measurements (total organic carbon (TOC) = 0.32–5.4, with an average of 1.07, unpublished data) show that the organic matter contents in the strata are very high, which is beneficial for oil and gas formation. Four lithofacies can be identified in the Qiongzhusi shale: phosphorite sand dolomite, silty mudstone, siltstone, and quartzose sandstone (Figure 3).

Phosphorite sand dolomite is dark-colored and has high hardness; this lithofacies has high dolomite contents, and the dolomite metacrysts are subhedral rhombohedrum and subhedral-xenomorphic granular with an irregular distribution. Some microcrystalline dolomites are unevenly distributed as metasomatic residue, indicating that the crystalloblastesis was incomplete and that the metamorphic grade is epizonal. The lithofacies is rich in collophane, which is primarily present as chaotic and irregular occurrences. In this lithofacies, pyrite is common and primarily framboidal. This lithofacies is primarily developed in the lower and middle Qiongzhusi Formation (Figure 3).

Silty mudstone is laminated and has a dark color. Clay minerals are predominant along with minor amounts of quartz. A small amount of collophane detritus is irregularly distributed. This lithofacies is primarily developed in the middle-upper Qiongzhusi Formation (Figure 3).

Calcareous siltstone is laminated and has a grayish black color. The silt grains are primarily quartz with minor feldspar. The calcite matrix is characterized by a heterogeneous distribution of grain morphologies.

Dolomitic siltstone is dark-colored. The silt grains are largely quartz and tightly compacted, with a grain size ranging from 10 to 60 μm. The distribution of the iron and argillaceous matrix is chaotic.

4.2 Major and trace elements

The results of the major element analysis (Table 1) show that the SiO_2 contents are 50.94–65.06 wt%, with an

Table 1: Major (wt%) and trace element (ppm) analysis results for the Qiongzhusi Formation in the Mabian region

Sample Lithology	PM05–04 Carbonaceous sandstone	PM05–06 Black mudstone	PM05–08 Black siltite	PM05–10 Black siltite	PM05–14 Black siltite	PM05–15 Black siltite	PM05–16 Black siltite	PM05–18 Black siltite	PM05–19 Black siltite	D0505 Carbonaceous mudstone
Fe_2O_3	2.69	1.56	1.08	1.31	0.74	0.54	1.87	2.63	0.83	2.94
FeO	1.99	2.90	2.05	2.96	3.66	3.10	3.16	3.90	4.36	1.18
MgO	3.22	4.88	3.05	5.03	4.90	4.02	4.05	4.57	6.16	2.27
CaO	0.49	3.51	8.22	2.72	2.05	2.50	2.60	1.14	4.68	4.46
Al_2O_3	15.18	13.25	11.48	13.02	14.73	13.95	11.89	15.95	12.53	14.64
K_2O	6.48	5.53	3.53	3.96	5.13	4.98	4.34	5.24	4.30	6.43
Na_2O	0.66	0.88	2.04	1.53	1.47	1.80	1.15	0.17	0.07	0.15
P_2O_5	0.22	0.20	0.16	0.22	0.26	0.32	0.27	0.22	0.38	3.62
SiO_2	64.02	58.20	56.20	60.65	61.04	65.06	61.68	55.36	50.94	46.70
MnO	0.095	0.070	0.15	0.060	0.062	0.049	0.069	0.077	0.082	0.0048
TiO_2	0.83	0.67	0.48	0.60	0.75	0.75	0.76	0.84	0.73	0.76
CuO	0.0048	0.0041	0.0030	0.0035	0.0049	0.0011	0.0027	0.0053	0.0062	0.0010
LOI	4.09	8.23	11.46	7.89	5.07	2.84	8.05	9.73	14.86	16.73
Ba	648	526	517	453	515	525	569	576	492	1403
Cr	79.2	63.5	63.2	50.4	61.9	62.3	69.8	75.6	58.1	71.0
Ga	18.5	15.5	15.4	14.5	13.7	13.8	16.3	22.4	19.3	24.3
Sr	47.8	68.3	68.1	70.7	103	104	44	28.9	47.5	84.0
Th	9.34	7.19	7.18	8.38	10.3	10.5	10.9	12.4	9.41	8.43
U	2.51	2.80	2.71	2.30	1.50	1.51	3.45	4.57	2.17	23.5
V	130	132	131	87.4	75.9	76.7	146	205	140	1636
Co	18.8	11.4	11.6	9.96	9.20	9.09	12.3	15.6	13.6	4.93
Ni	71.8	41.0	41.1	31.4	24.1	24.2	43.7	66.2	50.9	68.6
As	12.2	37.1	36.8	10.4	2.93	2.94	18.60	21.9	7.87	54.2
Zn	73.7	81.4	80.9	45.9	30.1	30.2	79.6	92.3	58.4	142
Zr	97.4	68.8	68.5	76.5	29.4	29.6	58.9	164	72.7	81.9
Rb	118	99.6	99.2	89.3	75.6	75.7	113.2	149	121	211
Hf	3.20	2.02	2.01	1.99	1.13	1.15	2.11	4.61	2.28	2.44
CIA	63	48	50.	57	58	55	57	66	59	50
PIA	84	46	50	61	64	58	63	83	91	50
CIW	91	62	62	71	75	70	75	89	97	62

All the elements tested here were measured against standard values.

average of 59.77 wt%; the Al_2O_3 contents are 11.48–15.95 wt%, with an average of 13.66 wt%; the Fe_2O_3 contents are 0.54–2.94 wt%, with an average of 1.62 wt%; the FeO contents are 1.18–4.36 wt%, with an average of 2.93 wt%; the MnO contents are 0.0048–0.095 wt%, with an average of 0.07 wt%; the contents of CuO are 0.0010–0.062 wt%, with an average of 0.0037 wt%; and the TiO_2 contents are 0.48–0.84 wt%, with an average of 0.72 wt%.

The analyses show that the average Ba, Sr, U, Th, As, V, Co, Ni, and Zn contents are 622, 66.6, 4.70, 9.40, 20.49, 276, 11.65, 46.30, and 71.41 ppm, respectively (Table 1).

4.3 Rare earth elements

The rare earth element (REE) data are shown in Table 2. The ΣREE contents of the sedimentary rocks in the study area range from 98.88 to 393 ppm, with an average of 199 ppm, which is slightly lower than that of Post-Archean Australian Shale (PAAS) (212 ppm). These values also coincide with the gradual decrease in REE abundance in the sedimentary rocks according to the shale, sandstone, and limestone sequence [33–36]. All these samples are characterized by Σlight REE (ΣLREE)/Σheavy REE (ΣHREE) ratios >1 and La/Yb ratios >11.8 (Table 2). These samples are clearly enriched in LREEs and depleted in HREEs (Figure 8; Table 2).

5 Discussion

5.1 Analysis of sediment sources

5.1.1 Major elemental constraints

Bhatia and Crook [37] found that the major elemental compositions differ markedly among the siliciclastic rocks deposited in various tectonic environments, which is also true among the limestones [33]. Therefore, the major elemental results are used to determine the sources of the sediments of this study. The ratios of w (SiO_2)/w (Al_2O_3) in the analyzed samples range from 3.19 to 5.19, with an average of 4.29, which is slightly higher than that of the continental crustal average (3.6) [38], indicating that the sediments were primarily derived from continental clastic material [2–5]. The w (Al)/w (Al + Fe + Mn) ratios of the samples range between 0.62 and 0.72, with an average of 0.68, again indicating a continental sediment source [40–50]. Consequently, the sediments were sourced primarily from continental siliciclastics, and the ferromanganese input from hydrothermal fluids released from the seafloor was very limited. Additionally, the ratios of w (Si)/w (Si + Al + Fe) range from 0.73 to 0.81, with an average of 0.78, indicating that the sediments were primarily derived from clastic material, not affected by biological activity [26,50–52]. The log(SiO_2/Al_2O_3) vs log (TFe_2O_3/K_2O) diagram (Figure 4a) indicates that the sediments in this area are composed primarily of sandstones and minor shales, implying that the sediments were not transported for a long distance and sorted and that they have a moderate level of maturity. An analysis employing the discriminant functions F1–F4 by Roser and Korsch [53] (Figure 4c and d) showed that the primary provenance of this area is a quartzite sediment source, with very limited input from a felsic igneous source. The results show that there was a relatively stable material source during the depositional period of the Qiongzhusi Formation and that the mineral maturity of the parent rock was moderate. The Zr–TiO_2 diagram (Figure 4b) shows that the source region was largely detritus from neutral igneous rocks, resulting in high Ti contents; therefore, the source region was influenced by magmatism and was not a pure siliciclastic rock area.

The major elemental analysis indicates that the early Cambrian Qiongzhusi Formation in this area is primarily composed of a set of continental clastic materials with a stable provenance, moderate level of mineral maturity, and limited inputs from neutral-felsic igneous rocks and submarine hydrothermal fluids. The diagenesis process was not affected by obvious biological activity.

5.1.2 Trace elemental constraints

Studies on sediments show that the ratios of metal minerals with different characteristics can be used to identify sediments of different origins [33,40,43,45,54,55]. Our samples display high concentrations of five main low-temperature metallogenic elements, namely, Zn, Pb, As, Ag, and Sb, which were 1.0, 1.3, 11, 6.1, and 5.2 times higher, respectively, than the standard crustal values [38]. The enrichments in these elements may be related to enrichments in organic matter [24]. The average Ba and Zn contents in the samples are 1.46 and 1.02 times higher, respectively, than those of the standard crustal values, indicating a weak hydrothermal influence [56]. The Ba/Sr ratios of the samples range from 5.0 to 20, with an average of 11, indicating the influence of submarine hydrothermal fluids

Table 2: The REE (ppm) analysis and calculation results for the Qiongzhusi Formation in the Mabian region

Sample	PM05–04	PM05–06	PM05–08	PM05–10	PM05–14	PM05–15	PM05–16	PM05–18	PM05–19	D0505
Lithology	Carbonaceous sandstone	Black mudstone	Black siltite	Black siltite	Black siltite	Black siltite	Black siltite	Black siltite	Black siltite	Carbonaceous mudstone
La	43.8	18.26	26.75	29.4	35.9	36.3	71.3	96.3	38.1	53.9
Ce	38.36	16.08	47.46	16.7	29.4	74.52	44.1	68.2	30.7	21.6
Pr	6.14	2.96	6.62	3.28	4.6	8.35	9.34	15.1	6.07	3.94
Nd	25.56	11.64	27.5	12.7	20.7	32.91	38.4	65.7	25.2	14.6
Sm	5.32	2.57	5.86	2.09	4.6	6.16	5.76	10.1	4.16	1.85
Eu	3.37	1.46	1.26	0.57	2.4	1.28	1.32	2.64	1.08	0.59
Gd	7.89	3.25	5.5	2.49	6.12	5.65	6.47	11.4	4.74	2.14
Tb	1.14	0.48	0.79	0.37	0.96	0.87	0.95	1.63	0.76	0.39
Dy	7.08	3.04	4.43	2.46	5.56	4.93	5.54	8.58	4.36	1.77
Ho	1.75	0.76	0.86	0.58	1.34	1.03	1.26	1.74	0.94	0.35
Er	4.59	1.75	2.45	1.64	3.54	3.02	3.34	4.56	2.65	1.14
Tm	0.67	0.26	0.34	0.28	0.46	0.44	0.43	0.54	0.35	0.13
Yb	2.87	1.15	2.26	1.19	2.17	2.9	2.15	2.45	1.79	1.86
Lu	0.46	0.28	0.33	0.19	0.37	0.46	0.36	0.34	0.25	0.15
Y	95.32	34.94	28.5	35.6	75.65	30.99	83.4	104	52.1	29.6
ΣREE	244.32	98.88	160.91	109.54	193.77	209.81	274.12	393.28	173.25	134.01
ΣLREE/ΣHREE	1.0	1.2	2.5	1.4	1.0	3.2	1.6	1.9	1.6	2.6
Eu/Eu*	0.51	0.50	0.22	0.25	0.45	0.22	0.22	0.25	0.24	0.30
Ce/Ce*	1.5	1.5	2.8	1.0	1.4	3.3	1.1	1.2	1.4	0.75

Eu* = Eu/(0.5 × (Sm + Gd)). Ce* = Ce/(0.5 × (La + Pr)). All the elements tested here were measured against standard values.

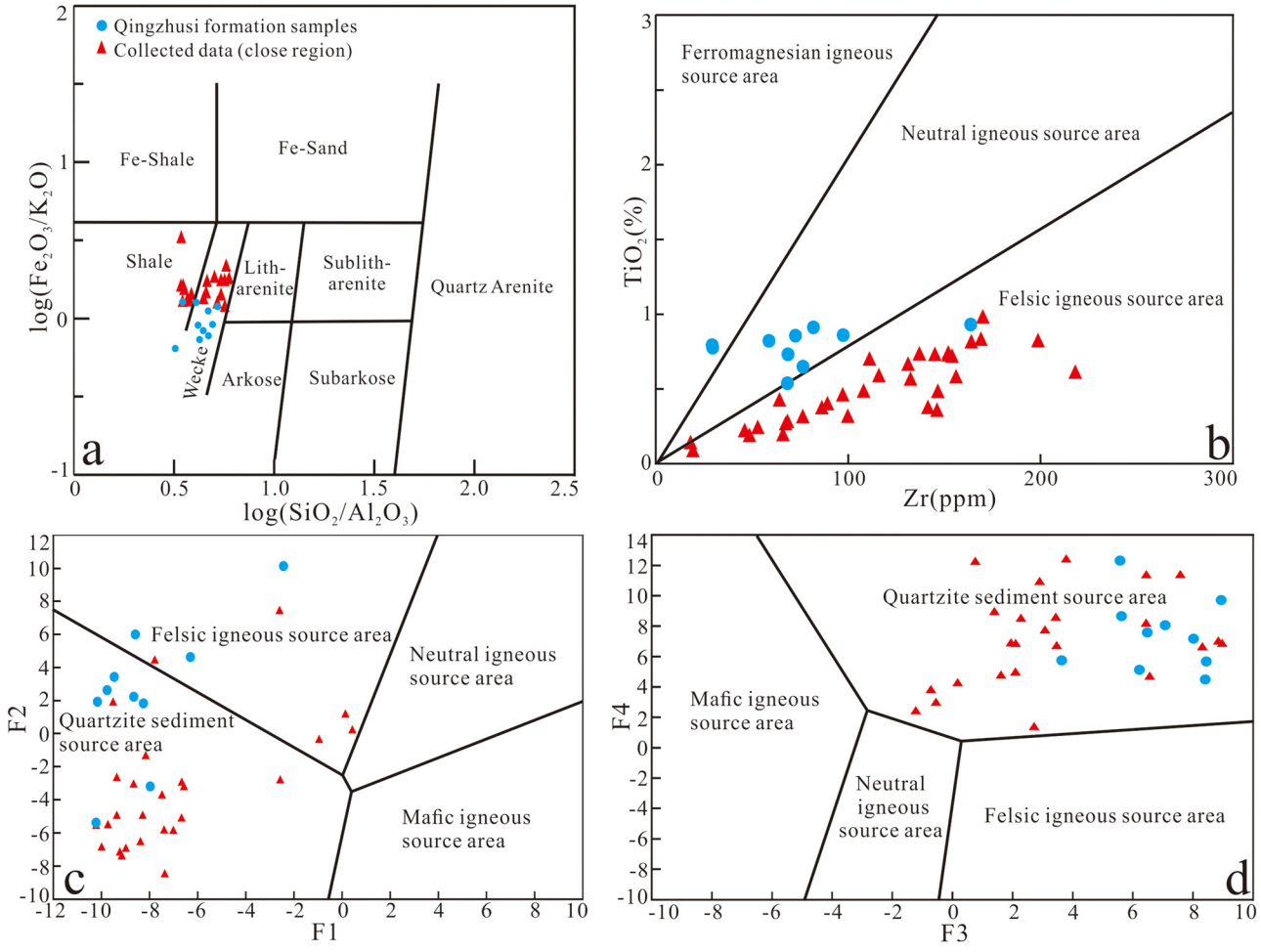

Figure 4: Source region discrimination based on principal element analysis (the discriminant function formulas are as follows: F1 = –1.773TiO_2 + 0.607Al_2O_3 + 0.76TFe_2O_3 – 1.5MgO + 0.616CaO + 0.509Na_2O – 1.224K_2O – 9.09; F2 = 0.445TiO_2 + 0.07Al_2O_3 – 0.25TFe_2O_3 – 1.142MgO + 0.438CaO + 4.75Na_2O + 1.426K_2O – 6.861; F3 = 30.638TiO_2/Al_2O_3 – 12.541TFe_2O_3/Al_2O_3 + 7.329MgO/Al_2O_3 + 12.031Na_2O/Al_2O_3 + 35.402K_2O/Al_2O_3 – 6.382; F4 = 36.500TiO_2/Al_2O_3 – 10.879TFe_2O_3/Al_2O_3 + 30.875MgO/Al_2O_3 – 5.404Na_2O/Al_2O_3 + 11.112K_2O/Al_2O_3 – 3.89) (a and b), the distinguishing criteria are in accordance with [27]; (c and d), the distinguishing criteria are in accordance with [53].

during the deposition [57,58]. High contents of Ba, As, and U are also an important indicator of submarine hydrothermal deposition [59,60]. The Ba, As, and U contents of the samples are 1.46, 11.38, and 1.74 times higher, respectively, than those of the upper continental crust (UCC). These findings show that the Qiongzhusi Formation was influenced by submarine hydrothermal fluids during the deposition.

The Co/Zn ratios of the samples are between 0.035 and 0.31, with an average of 0.20, showing that this area experienced weak hydrothermal deposition [56]. In this paper, all the samples plot in the hydrothermal deposition field with the covariation relation of Co/Zn–(Cu + Co + Ni) (Figure 5a), suggesting that the Qiongzhusi Formation in the Mabian area was significantly affected by hydrothermal activity [48]. Studies reveal that Cr is primarily derived from terrestrial clastic material [35,36] and has no obvious correlation with Zr because deposition and accumulation will occur without the transfer of elements such as Zr under the influence of hydrothermal fluids [61]. Our analyses of the Qiongzhusi samples do not have a correlation between Cr and Zr (Figure 5b), indicative of a likely influence of hydrothermal activity on the seafloor. The Co–Ni–Zn ternary diagram (Figure 6) also shows that the sample collection area was affected by hydrothermal activity during the deposition of the Qiongzhusi Formation, and the low ratios of Th/Sc (0.54–0.99, with an average of 0.74; the UCC has a ratio of 1) and Th/U (0.36–6.97, with an average of 3.70; the UCC has a ratio of 3.8) indicate that the deposition of the Qiongzhusi Formation coincided with the extensional rift period in the Yangtze Block [28,58,62]. Many scholars believe

that the formation of extensional rifts in the crust is an important factor in generating anomalies within the elemental geochemical system in sediments [26,35,52,63]. This finding clearly shows that the sediments in the Mabian area were influenced by seafloor tectonics during this period. The source region had not undergone multiple rounds of sedimentary recycling, as shown in Figure 5c and d. Thus, the chemical composition changes directly reflect the composition of the elements in the source region. Consequently, as shown in Figure 5e and f, the clastic material in the Qiongzhusi Formation was primarily derived from a continental sediment and influenced by a neutral-acidic igneous source associated with active tectonism, and the maturity was moderate.

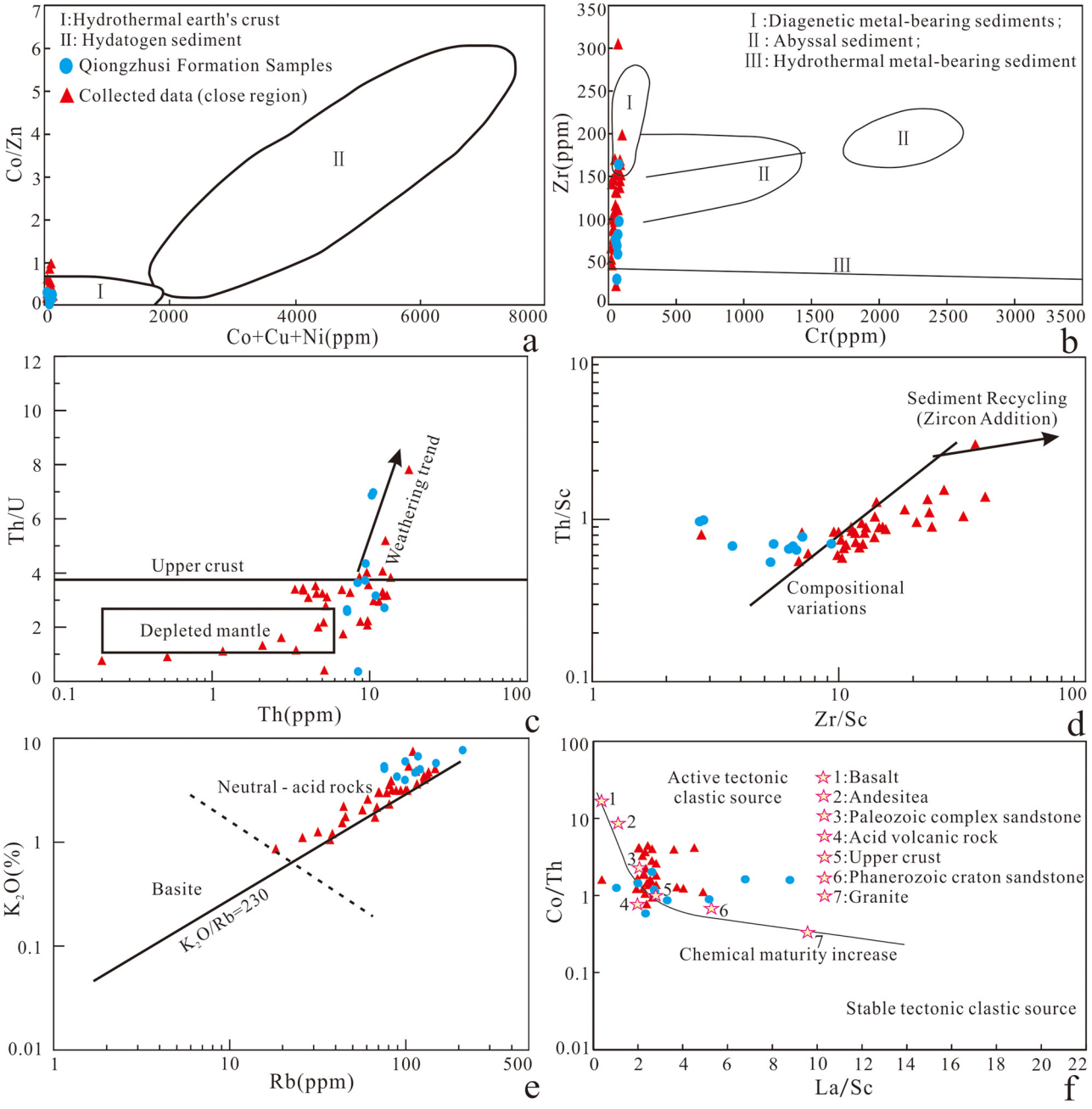

Figure 5: Trace element analysis of sediment sources. (a) Co/Zn–Co + Ni + Cu covariant graph; (b) Cr–Zr covariant graph (the c and d base map comes from ref. [56]); (c) Th–Th/U covariant graph; (d) Zr/Sc–Th/Sc covariant graph (the e and f base map comes from ref. [64]); (e) Rb–K covariant graph (the base map comes from ref. [65]); and (f) La/Sc–Co/Th covariant graph (the base map comes from ref. [59]).

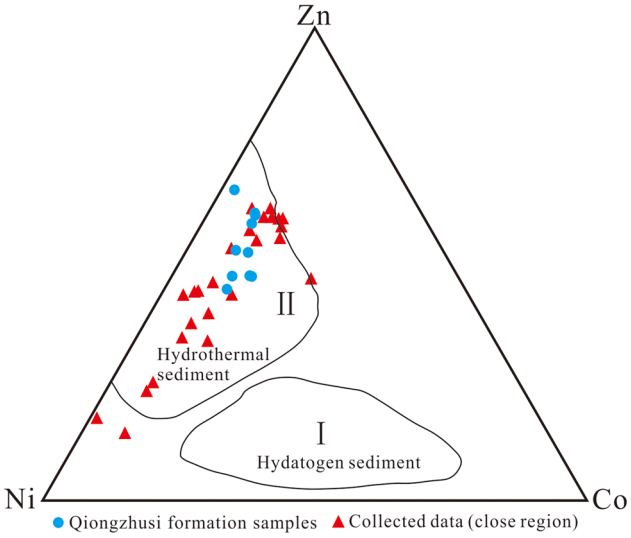

Figure 6: Co–Ni–Zn triangular chart (the base map comes from ref. [48]).

5.1.3 Rare earth element analysis

In general, the geochemical properties of REEs are relatively stable and rarely affected by various epigenetic processes; therefore, they can be used to indicate the depositional environment and material sources of sediments [62,66]. Chondrites are used to standardize the REEs in this paper. Additionally, Ce, Eu, and Pr anomalies are calculated via weighted average methods relative to adjacent elements [20]. The total REE values of the samples (an average of 199.19 ppm) in the study area are slightly lower than those in the PAAS (211.78 ppm) [67,68]. This finding indicates that the black rock series in the Qiongzhusi Formation is primarily continental, although it may have been influenced by seawater or hydrothermal fluids during the deposition process [35]. The ΣLREE/ΣHREE ratios range from 1.0 to 3.17, with an average of 1.80, which shows a relative enrichment in LREEs. Standardizing the pattern relative to chondrites (Figure 8c) clearly shows a right-dipping pattern, which is basically consistent with the UCC and PAAS standards and shows that the source region of the sediments was largely a continental clastic source. However, the Eu and Ce anomalies were primarily influenced by seafloor hydrothermal fluids, which is consistent with the results of the major and trace element analysis, while the negative Eu anomalies (0.22–0.51, with an average of 0.31) and

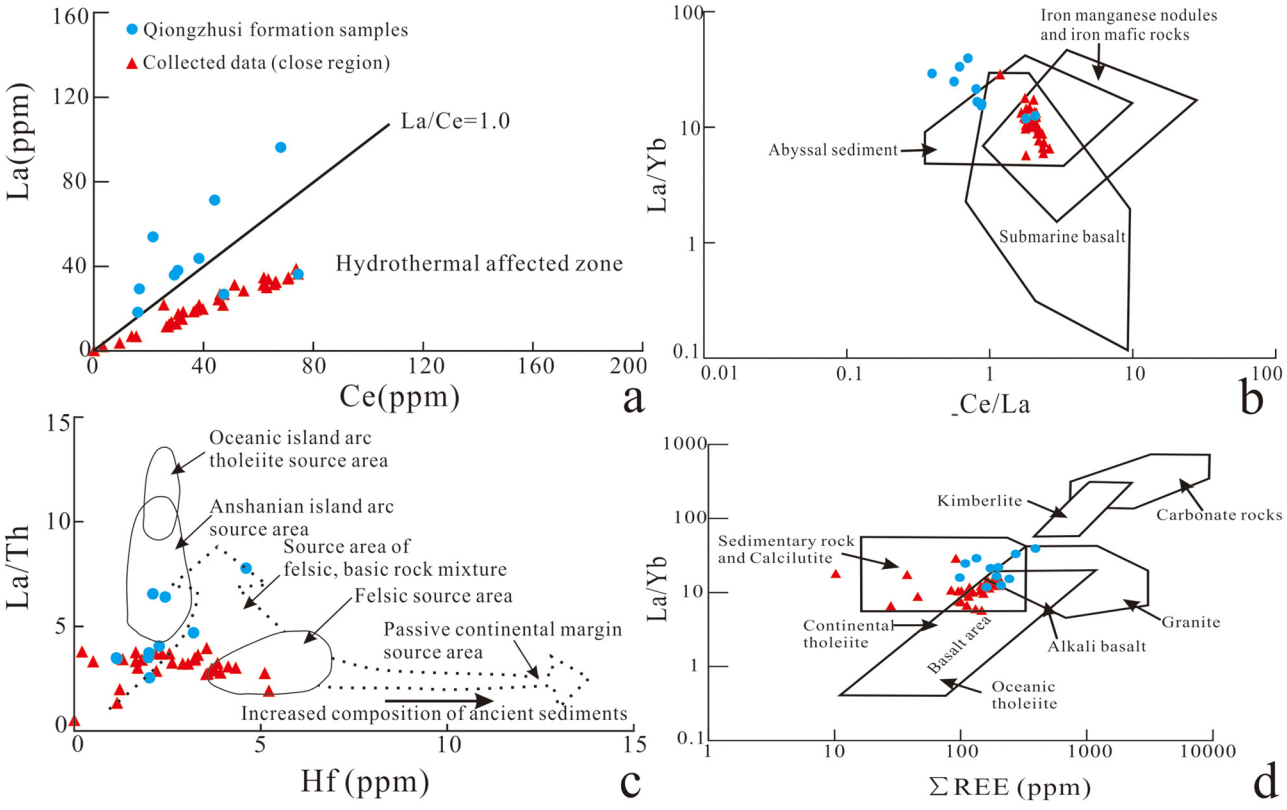

Figure 7: Rare earth element analysis of sediment sources. (a) Ce–La covariant graph (the base map comes from ref. [21,73]); (b) Ce/La–La/Yb covariant graph (the base map comes from ref. [72]); (c) Hf–La/Th covariant graph (the base map comes from ref. [65]); and (d) ΣREE–La/Yb covariant graph (the base map comes from ref. [73]).

the positive Ce anomalies (0.75–2.84, with an average of 1.62) were mostly controlled by the influence of the continental source region and the seafloor reducing environment. These conditions also illustrate that the black rock series of the early Cambrian Qiongzhusi Formation in the study area had both hydrothermal and normal seawater involvement [62]. Based on the La–Ce and La/Yb–Ce/La diagrams, the samples in this area are all from areas with a given influence from submarine hydrothermal fluids and submarine basalt (Figure 7a and b). The material composition of the source region can be determined from the La/Th–Hf and La/Yb–ΣREE diagrams (Figure 7c and d). The samples largely plot within the sedimentary rock and felsic-basic mixture rock. This finding also coincides with the uplift of the Kangdian ancient land to the west at that time [8,11,24,69,70].

5.2 Sedimentary environment

5.2.1 Identification of reducing and oxidizing environments

The spider diagrams of the major and trace elements show that the samples are weakly enriched in MgO, TiO_2, and P_2O_5 and depleted in Na_2O (Figure 8a), which reflects the effect of the enrichment of organic inputs on the samples during diagenesis [74]. The high contents of P_2O_5 and ΣREE indicate that the enrichment of organic inputs here may have been affected by an upwelling ocean current [11,12,69,75]. Phosphate is a biochemical deposit that occurs in dry climates, and a high abundance of phosphate is consistent with the early tidal facies of the Qiongzhusi Formation in this area, which is rich in colloidal phosphate rock. In addition, the area of greatest phosphate ore enrichment should have been located in the lagoon area behind the tidal shoal, which is consistent with the location of the main phosphate ore-producing areas in the Mabian area [76,77]. The trace element compositions show obvious positive anomalies for V and Ni, slight positive anomalies for Sc and Cr, obvious negative anomalies for Sr and Hf, and slight negative anomalies for Zr and Nb, which reflect the influence of the source region on the samples [52,67,78]. The Al, Ti, and Th contents of the samples are very similar to those of the UCC, indicating that they were supplied from continental clastic material [79,80] (Figure 8a and b). The negative Sr anomaly in these samples is derived from the continental source region [81]. During the diagenesis stage, the disturbance by submarine hydrothermal fluids

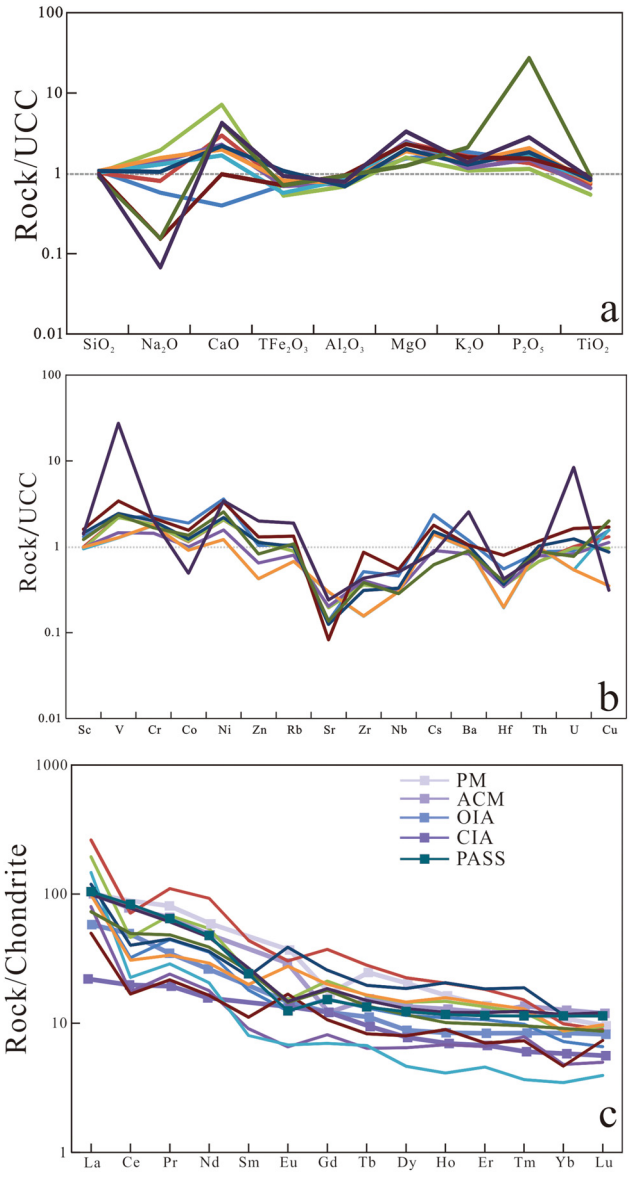

Figure 8: (a) Upper continental crust (UCC)-normalized major elements of the samples from the Shashi Formation; (b) UCC-normalized trace element spidergrams of samples from the Shashi Formation. The normalized values of UCC are from ref. [38]; (c) chondrite-normalized REE patterns of the samples from the Shashi Formation. The normalized chondrite values are from ref. [38]; and PAAS, PM, ACM, OIA, and CIA are from ref. [37]. The symbols in a and b are the same as those in c.

affected the elemental compositions and resulted in the substitution of V and other elements in the marine facies. Last, the changes led to some anomalies in the major and trace elements of the Qiongzhusi Formation. Previous studies have suggested that trace elements, such as Mo, V, U, and Mn, can be used to distinguish the redox conditions of marine sediments because they are sensitive indicators of paleoceanographic processes [40,82–84].

Hatch and Leventhal [85] and Jones and Manning [34] asserted that the redox environment can be distinguished based on these indicator elements, and they proposed a comprehensive criterion (Table 3). We calculate that the V/(V Ni) (0.64–0.96, average of 0.76) and V/Sc ratios (7.1–106, average of 19) indicate an anaerobic environment; the V/Cr ratios (1.2–23, average of 4.0) indicate an oxygen-poor environment; and the Ni/Co (2.62–13.928, average of 4.5), U/Th (0.14–2.78, average of 0.53), and δU ratios (0.60–1.79, average of 0.98) indicate an oxygen-enriched environment. However, these values are located near the oxygen-poor environment field and do not vary significantly. Our observations show an enrichment in U, V, and Mn and a lack of enrichment in Ni and Cu, which indicates that the anoxic sedimentary environment was caused by the stratification of seawater and slow O_2 regeneration in deep water [80,86]. This finding also indicates that the water body in the Mabian area may have been impacted by upwelling ocean currents, which promoted marine productivity, and the anoxic reducing environment was conducive to the preservation of organic matter. The curve of the redox parameters over time shows that the redox environment was clearly affected by the climate because the chemical index of alteration (CIA), chemical index of weathering (CIW), and plagioclase index of alteration (PIA) values decreased as the climate became hot and dry. The redox parameters in the profile initially tend to reflect an oxidizing environment, and when the climate became warm and humid, the redox parameters tend to reflect a reducing environment. However, P_2O_5, which is affected by upwelling ocean currents, increased in abundance. The increase in the P_2O_5 content indicates the formation of the upwelling ocean current. Subsequently, the climate became warm and humid, and the sedimentary environment became reducing. Consequently, the deposition of the Qiongzhusi Formation in the Mabian area was clearly influenced by upwelling ocean currents. In addition, upwelling ocean currents played a vital role in the paleoclimatic environment of the region (Figure 9).

5.2.2 Reconstruction of the degree of weathering of the deposits

The paleoclimate can be reconstructed by using the CIA, CIW, and PIA [50,74,87,88] as well as the trace element ratios of Sr/Cu and Rb/Sr [51,78,88,89]. The chemical compositions of sedimentary clastic rocks are commonly affected by weathering and diagenesis, which may obscure the elemental characteristics of the original compositions [87,90,91]. The CIA is a chemical index that is used to determine the degree of chemical weathering in the source region ($CIA = [Al_2O_3/(Al_2O_3 + CaO^* + Na_2O + K_2O] \times 100$), principal components are mole fractions, CaO* is only the CaO in silicate and represents the mole fraction of CaO of the whole rock minus the CaO of chemically deposited rock). Based on this equation, the CIA values (52–72, average of 60) of the sampled sequence correspond to weak to moderate weathering. Furthermore, the other calculated indices, CIW (63–98, average of 80) and PIA (50–97, average of 71.92), show that the overall degree of weathering is moderate. These results are consistent with the general trend in the sedimentary profile from tidal facies to continental shelf facies and the accumulation of colloid phosphate deposits in the early strata. The chemical weathering degree and potassium metasomatism were characterized using the A–CN–K ternary diagram in addition to the CIA, CIW, and PIA

Table 3: Trace element depositional environment discrimination

		Anoxic environment		Oxygen-enriched environment
Type		**Anaerobic**	**Oxygen poor**	
V/(V + Ni)		>0.50	0.46–0.60	<0.46
V/Cr		>4.25	2.00–4.25	<2.00
V/Sc			>7.90	<7.90
Ni/Co		>7.00	5.00–7.00	<5.00
U/Th		>1.25	0.75–1.25	<0.75
Au [ppm]		>12.0	5.00–12.00	<5.00
δU			>1	<1
Paleogeographic environment		Low energy, viscous flow, limit, upwelling		High energy, circulation unimpeded
Paleontology	Benthonic animal	Lack	Soft organism development	Thriving
	Biodisturbance	Non	Absence–usual	Intense

Note: $\delta U = 2 \times U/(U + Th/3)$.

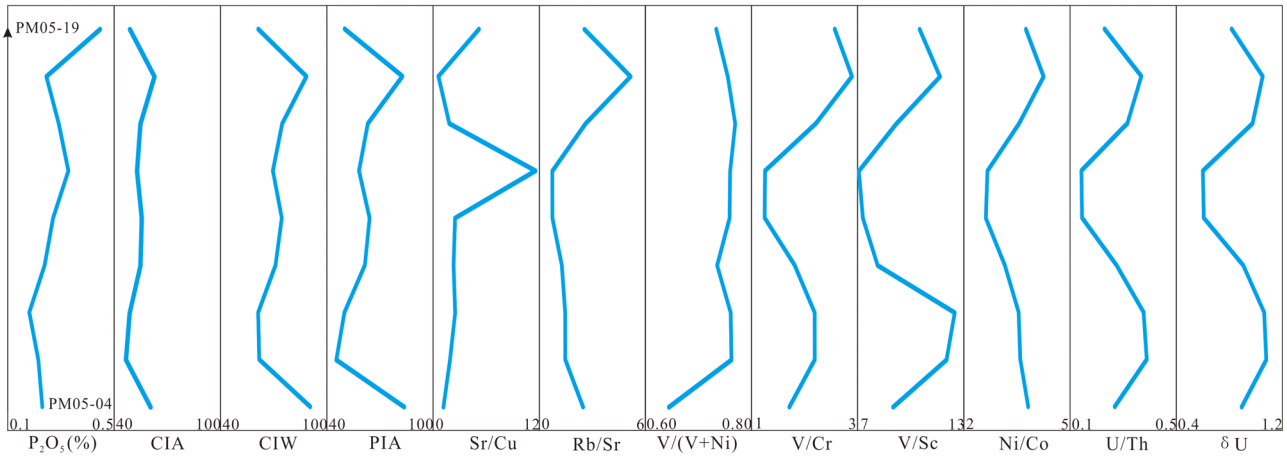

Figure 9: Variation curves of the weathering index and the redox index in the Qiongzhusi profile.

[74,87,90]. Based on the results, plagioclase was dominant during the early stage of chemical weathering (Figure 10), Ca and Na disappeared rapidly, and the weathering product was illite. Montmorillonite and kaolinite are characterized by an evolutionary trend line parallel to the A–CN line. After the disappearance of plagioclase, biotite, potassium feldspar, and illite began to be weathered and K was released from these minerals during the moderate weathering stage. In the late stage of chemical weathering, the secondary clay was characterized by kaolinite, gibbsite, and chlorite, and the combination of weathering products was close to point A [74]. After correction for K metasomatism, the samples mostly plot within the moderately weathered and strongly weathered areas (only two samples, PM0506 and PM0508, plot in the primary weathering zone). These results further indicate that the climate gradually shifted from dry and hot to moist and warm during this time (Figure 10). Nesbitt and Young [91] found that the CIA primarily exhibits moderate to strong weathering in tropical and subtropical regions, and the Cambrian Yangtze Block was located in a low-latitude tropical climate based on global paleogeography. The Sr/Cu ratios of samples are 0.68–12 (average of 3.8), indicating a humid climate [41,92]. However, the Rb/Sr ratios of the samples are 0.73–5.2 (average of 2.1), which are much higher than that of the PAAS [36], indicating warm and humid climate conditions [28,29,58,88]. Therefore, the depositional environment of the Cambrian Qiongzhusi Formation in the Mabian area was characterized by warm and humid climatic conditions, which were conducive to the Formation of organic matter.

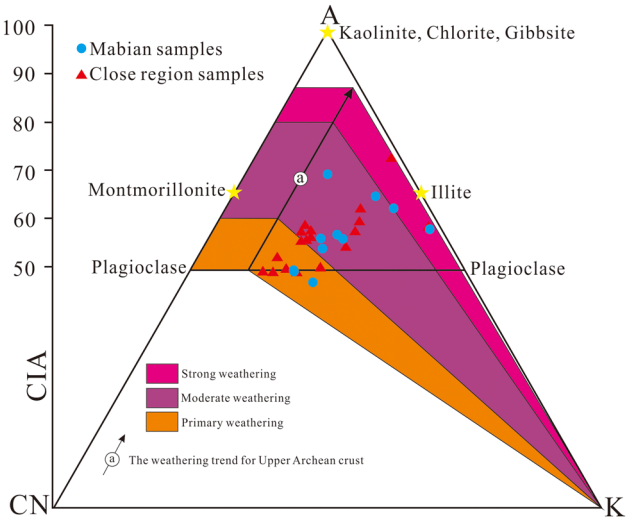

Figure 10: CIA weathering degree recovery (base map comes from ref. [78]).

The X-ray diffraction (XRD) analysis of previous studies on the drill core samples from the Qiongzhusi Formation [93] shows that the sediments are primarily composed of quartz and clay minerals. The average quartz content of the Qiongzhusi Formation is 34 vol% and can be as high as 44.5 vol%, and the clay mineral content of the Qiongzhusi Formation ranges from 6.7 to 64.2 vol%. X-ray fluorescence (XRF) analysis shows that the most abundant clay mineral in the Qiongzhusi Formation is illite, accounting for 68.3 vol%, followed by chlorite and illite-smectite mixed-layer minerals, and that the least abundant clay mineral is kaolinite. The above results also supported the sedimentary weathering intensity analysis, suggesting that the Qiongzhusi Formation is generally more than moderately weathered.

The above analysis indicates that the Cambrian Qiongzhusi Formation in the Mabian area formed in a warm and humid environment with weakly oxidizing to

weakly reducing water conditions associated with water stratification, which likely indicate the effect of upwelling ocean currents. The analysis of the samples from the study section and the ratios of elements show that the entire process consisted of the gradual deepening of the seawater and the relatively special nature of the Qiongzhusi Formation in the Mabian area because of its geographical location. The sedimentary facies show that this area was located in a transitional zone between coastal facies and shallow marine facies. When the transgression occurred, the sedimentary facies transitioned to shallow marine facies, and when the regression occurred, the sedimentary facies transitioned to shoreline marine facies, which resulted in changes in the geochemical properties of the sediments [13,37,40,81].

5.2.3 Sedimentary-tectonic environment

The samples mostly plot within the island arc and active continental margin fields (Figure 11). Samples with moderate quartz contents, which represent complex active margins and island arc environments, may also reflect regional material sources (which are deposited in extensional basins) related to strike-slip faults and are generally associated with relatively complex active structures [53]. This scenario is also similar to the Kangdian continental background. The $Al_2O_3/[Al_2O_3 + Fe_2O_3]$ ratios of the samples in this study are between 0.833 and 0.963, with an average of 0.90, indicating that most of the samples were deposited in a continental margin environment [94]. Banerjee and Prosun [95] proposed that the tectonic environment during deposition can be determined by using the relationship among TFe_2O_3, MgO, TiO_2, Al_2O_3, and SiO_2. In the diagram (Figure 11a and b), most of the data plot within the island arc tectonic area. This area primarily reflects high Ti contents, which are influenced by hydrothermal fluids in the source region analysis. The $\log(K_2O/Na_2O)$ vs SiO_2 diagram (Figure 11c) also points to a continental margin facies, which is primarily associated with island arcs and tectonically active areas [53,96]. The TFe_2O_3/TiO_2 and $Al_2O_3/Al_2O_3 + Fe_2O_3$ (Figure 11d) bivariate plans also indicate that the samples were deposited in a continental margin depositional environment. The MnO/TiO_2 ratios are mostly within the range of 0.07–0.31, with an average of 0.108, which is clearly less than the threshold value of 0.5, indicating that the depositional area was located in a continental slope and marginal marine environment [89].

The Qiongzhusi Formation was deposited in a turbulent continental margin facies zone associated with an island arc, and these conditions had an important effect on the elemental changes during the depositional period of the Qiongzhusi Formation.

The samples in this study plot from the continental arc and active continental margin fields in the discriminant diagrams of Th–Co–Zr/10 (Figure 12a) and Th–Sc–Zr/10 (Figure 12b) are consistent with the results of the major element discriminant diagram (Figure 11c), although a large number of points are located in the low Zr/10 region. This result is largely due to the decrease in Zr content that occurs during diagenesis [39,40,45] in the marine environment. If the diagenetic interference from Zr is excluded, most of the points plot within the active continental margin field. The La/Y–Sc/Cr and La–Th diagrams (Figure 12c and d) further confirm that the Qiongzhusi Formation in the Mabian area was likely deposited in a relatively active continental margin. The diagram also indicates a turbulent environment during the depositional period and the disturbance of the seafloor by the water body.

REE-based tectonic discrimination mostly focuses on the continental arc, island arc, active continental margin, and passive continental margin environments. The points mostly plot within the continental arc field (Figure 13), which further shows that the area was influenced by a continental arc during the deposition of the Qiongzhusi Formation. This influence was especially prominent during the transgressive period of the Qiongzhusi Formation deposition. An oceanic plate was subducting beneath the continent at this time, and the Kangdian ancient land to the west of the Mabian area was the site of plate collision [12,13,20]. Consequently, the elemental geochemistry of the Qiongzhusi Formation in this area reflects continental arc and continental margin characteristics. This result also coincides with the overall geological background. The related REE and trace element diagrams are also consistent with the abovementioned ternary diagram (Figure 12).

5.3 Sedimentary environment analysis

The black rock series of the lower Cambrian Qiongzhusi Formation in southern China is primarily a product of tectonic activity, hydrothermal activity, and anoxic conditions [13,21,71]. The presence of Fe-rich and magnesium-rich deep-sea sediments usually indicates a tectonic setting involving lithospheric extension [62,93,86]. Chen et al. [75] concluded that the lithospheric extension associated with the early Cambrian Qiongzhusi

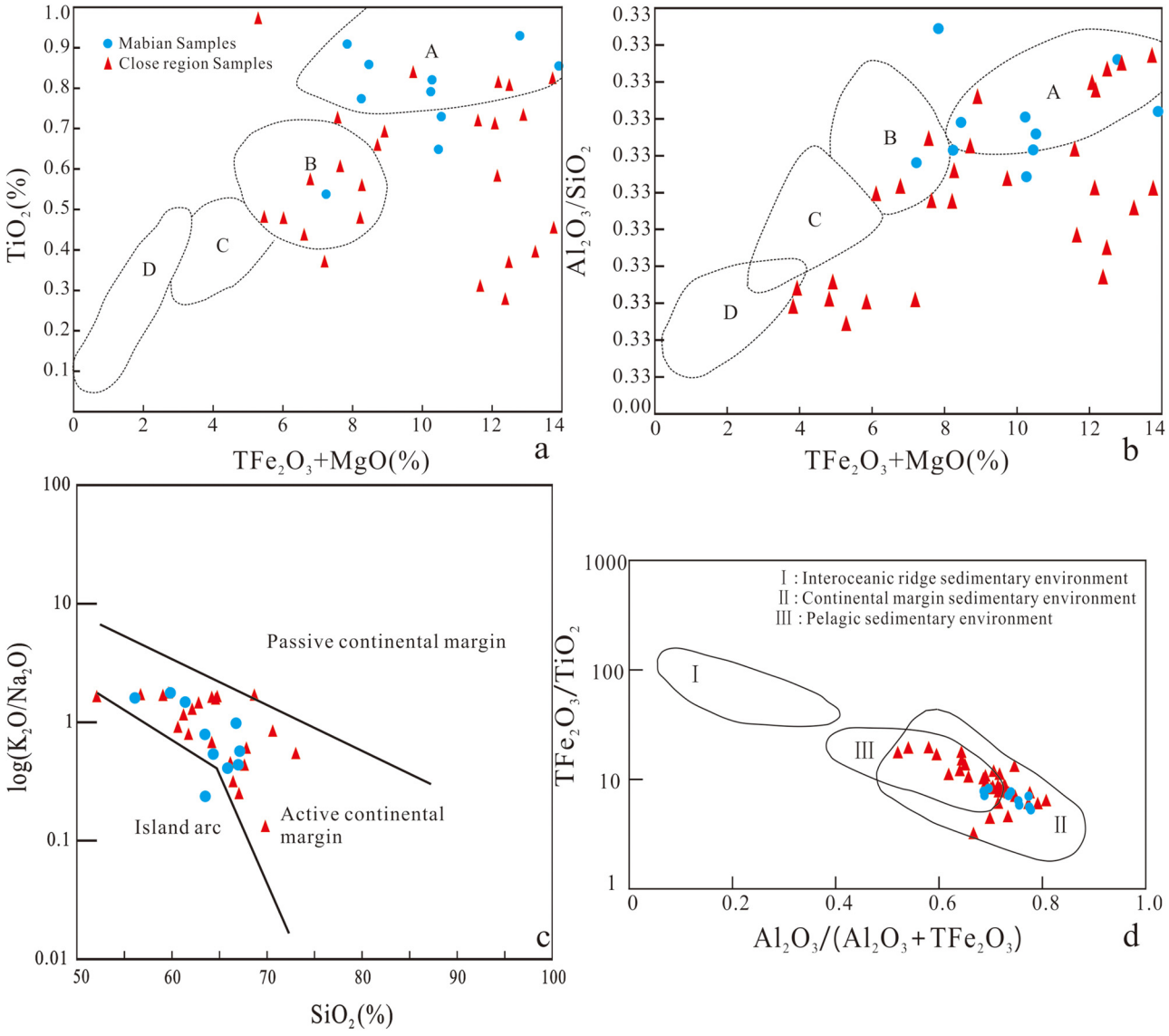

Figure 11: Identification of sedimentary tectonic environment by principal elements. (a) TFe_2O_3 + MgO–TiO_2 structural discrimination; (b) TFe_2O_3 + MgO–Al_2O_3/SiO_2 structural discrimination (a, b the base map comes from ref. [97]); (c) SiO_2–log(K_2O/Na_2O) structural discrimination (the base map comes from ref. [96]); and (d) $Al_2O_3/(Al_2O_3 + TFe_2O_3)$–$TFe_2O_3/TiO_2$ structural discrimination (the base map comes from ref. [94]). The diagrams are as follows: (A) oceanic island arc; (B) continental island arc; (C) active continental margin; and (D) passive continental margin.

Formation can be characterized as curtain extension (that is, the extension was rapid during the early stage and then slowed). During the Sinian and Cambrian, a large number of paleohydrothermal vents developed in the deep- and shallow-sea areas of the Mabian area [99,100]. Many stages of submarine volcanic eruptions and intrusions occurred along large deep faults [70,98,101], and material from deep heat sources mixed with surface water, groundwater, and seawater to form hot brines at various temperatures, leading to hydrothermal circulation and hydrothermal activity [102,103]. During the process of active hot brine circulation, elements in the basic and ultrabasic rocks of the Proterozoic Wuling Formation were dissolved in large quantities, and an ore-bearing hot brine formed. This process resulted in the syndepositional enrichment of some metal elements in the black rock series of the Cambrian Qiongzhusi Formation. Additionally, due to the effect of upwelling ocean currents, large amounts of nutrients were brought to the stagnant slope of the platform margin, resulting in the proliferation of abundant algae and plankton in the surface water and the Formation of large amounts of collophane deposits in this area. The

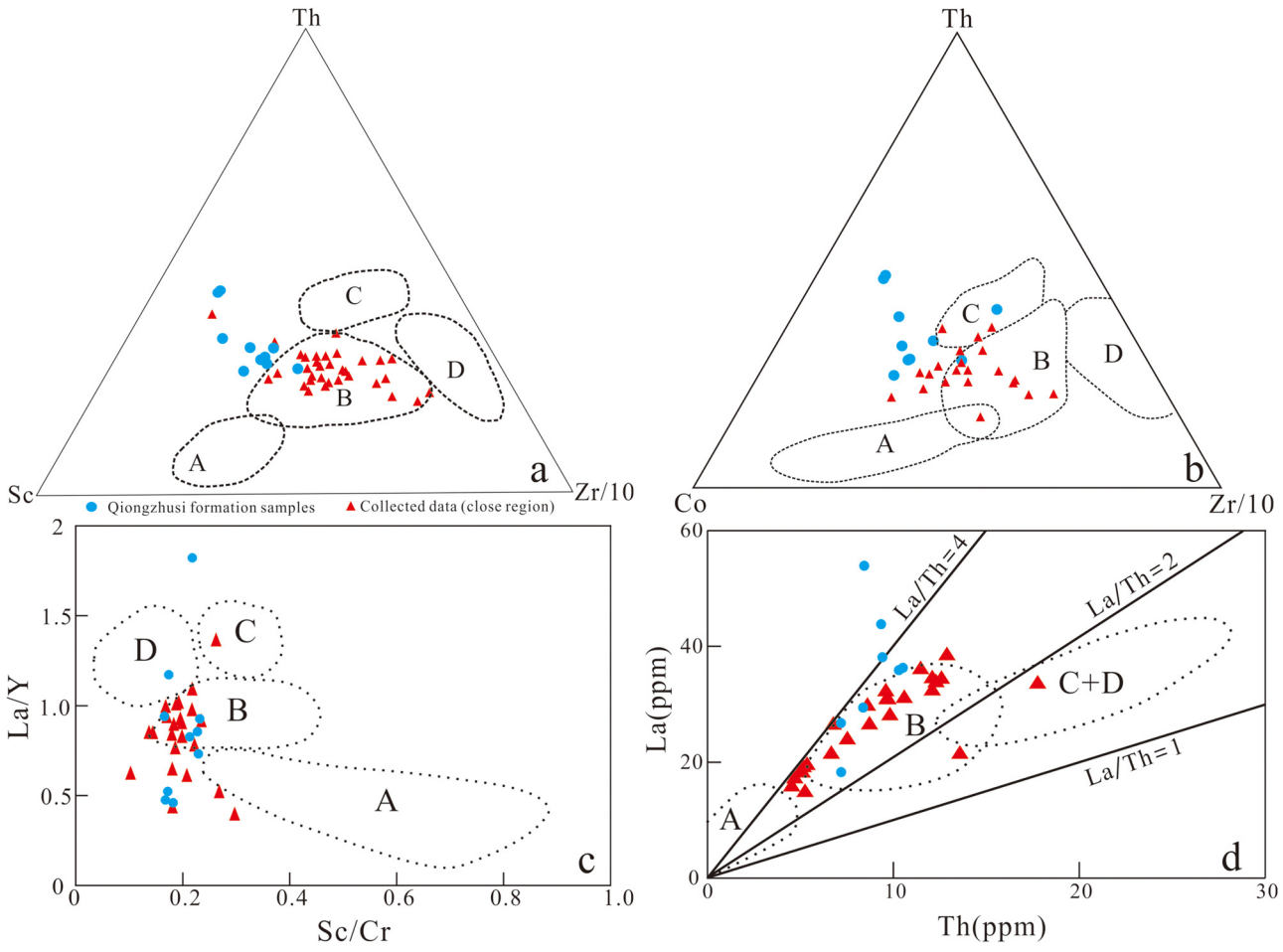

Figure 12: Identification of the sedimentary tectonic environment of the trace elements. The diagrams are the same as those in Figure 11a–d; the base map comes from ref. [97].

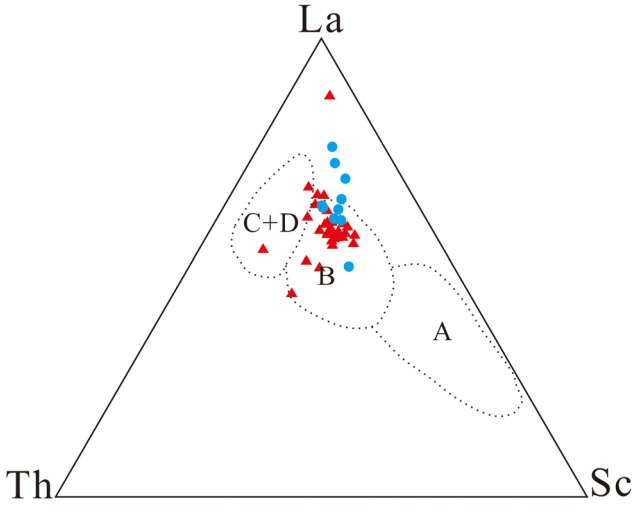

Figure 13: La–Th–Sc structural discrimination. The diagrams are the same as those in Figure 10; the base map comes from ref. [98].

high biological productivity and the abundance of biological organisms sinking after death provided abundant organic matter to the seabed, and the decomposition of the organismal remains consumed a large amount of dissolved oxygen. Oxygen regeneration in the deep water was slow at that time, and the high degree of dissolved oxygen consumption along the slope led to water stratification and an anoxic reducing environment. This environment was favorable for the preservation of organic matter in the black rock series. Therefore, a large amount of organic matter and phosphorus precipitated from the water column in the Mabian area during that time (Figure 14).

6 Conclusions

1) The early Cambrian Qiongzhusi Formation was primarily deposited during a transgressive period; the lithofacies transitioned from tidal facies to shallow-

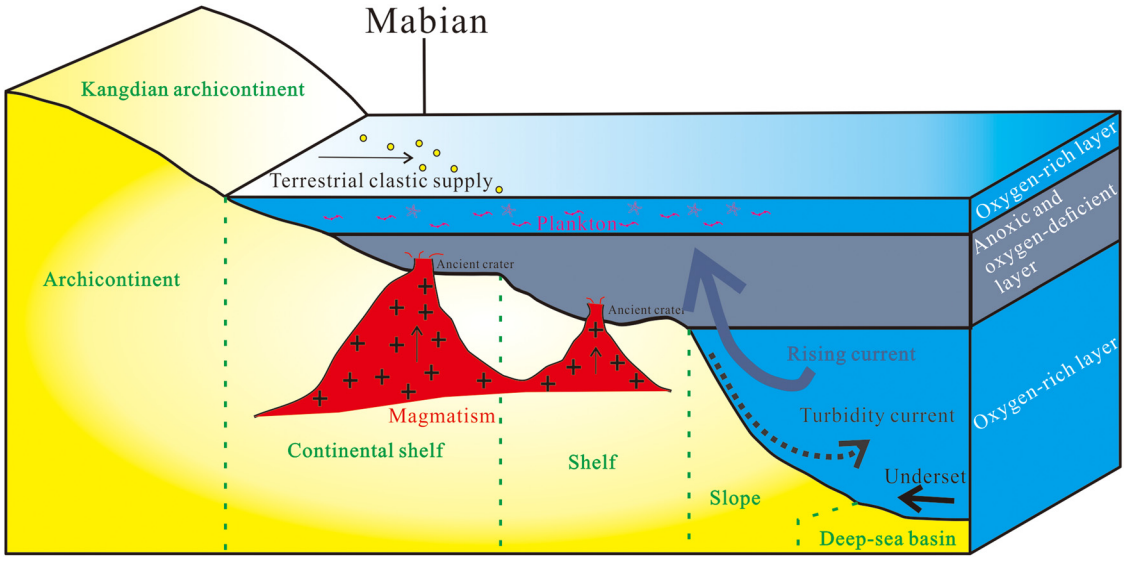

Figure 14: Environment of the Qiongzhusi Formation in the Mabian area.

sea shelf facies, and the types of sediment deposited gradually changed from fine clastics to muddy sediments according to field observations and laboratory analysis.

2) The sediment source region was thoroughly reconstructed, and the results indicated that the Qiongzhusi Formation received continental clastic material with neutral-acidic igneous rocks from a stable source and moderate maturity based on the analysis of major elements, trace elements, and REEs. Bioenrichment resulted in a substantial loss of Na_2O, and the influence of submarine hydrothermal fluids produced a large amount of Ti, V, and Ni enrichment during diagenesis.
3) A reconstruction of the paleosedimentary environment and depositional weathering intensity indicated that the depositional environment of the Qiongzhusi Formation consisted of a deep water body with anoxic conditions due to the stratification of the water body caused by upwelling in the Mabian area. However, an estimation of the weathering intensity via the CIA, CIW, and PIA showed that the climate of the Mabian area gradually changed from dry and hot to moist and warm during the deposition of the Qiongzhusi Formation. This change was also caused by the impact of a large amount of cold water from upwelling ocean currents on the regional climate.
4) The Yangtze Block experienced uplift and denudation in response to the Tongwan movement at the end of the Sinian during the deposition of the early Cambrian Qiongzhusi Formation. Additionally, a large-scale transgression occurred, and uplifted and subsided paleogeomorphology and extensional faults developed. In the context of this regional structure, the geochemical analysis primarily indicates that the whole area was in a continental slope and marginal marine environment associated with a continental arc tectonic system during the depositional period of the Qiongzhusi Formation, which is consistent with the petrological analysis of that section. In addition, the area was influenced by the Kangdian ancient land to the west.

Based on the summary of the four factors above, the lower Cambrian Qiongzhusi Formation in the Mabian area is concluded to have been deposited offshore under a moist and warm environment and was affected by submarine hydrothermal fluids in a continental arc tectonic system. This environment received a supply of neutral-acidic igneous rocks from Kangdian ancient land debris.

Acknowledgments: We are grateful to Mr Jianghong Deng and Mr Bin Deng for their assistance with the field survey. This study was financially supported by the China Geological Survey (subject No. 121201010000150004–08).

Author contributions: Hao Liu wrote the article, analyzed the data, and prepared the manuscript with contributions from all the co-authors. Chan Wang improved the manuscript and polished the English usage. Yong Li funded the study and made some improvements in the manuscript. Jianghong Deng and Bin Deng provided important

assistance in the selection of the research region and samples. Yuexing Feng, Hao Liu, and Chan Wang designed the experiments and Yuexing Feng performed them. Hui Chen, Yunlong Xu, and Shaoze Zhao drew the illustrations for this manuscript.

References

[1] Amthor JE, Grotzinger JP, Schröder S, Bowring SA, Ramezani J, Martin MW, et al. Extinction of Cloudina and Namacalathus at the Precambrian Cambrian boundary in Oman. Geology. 2003;31(5):431–4.

[2] Grotzinger JP, Bowring SA, Saylor BZ, Kaufman AJ. Biostratigraphic and geochronologic constraints on early animal evolution. Science. 1995;270(5236):598–604.

[3] Kaufman AJ, Jacobsen SB, Knoll AH. The Vendian record of Sr and C isotopic variations in seawater: implications for tectonics and paleoclimate. Earth Planet Sci Lett. 1993;120(3–4):409–30.

[4] Knoll AH, Carroll SB. Early animal evolution: emerging views from comparative biology and geology. Science. 1999;284(5423):2129–37.

[5] Brasier MD. Background to the Cambrian explosion. J Geol Soc. 1992;149:585–7.

[6] Marshall CR. Explaining the Cambrian "explosion" of animals. Annu Rev Earth Planet Sci. 2006;34(1):355–84.

[7] Maloof AC, Porter SM, Moore JL, Dudás FÖ, Bowring SA, Higgins JA, et al. The earliest Cambrian record of animals and ocean geochemical change. Geol Soc Am Bull. 2010;122(11–12):1731–74.

[8] Jin C, Li C, Algeo TJ, Planavsky NJ, Cui H, Yang X, et al. A highly redox–heterogeneous ocean in South China during the early Cambrian (~529–514 Ma): implications for biota–environment co-evolution. Earth Planet Sci Lett. 2016;441:38–51.

[9] Kimura H, Watanabe Y. Oceanic anoxia at the Precambrian–Cambrian boundary. Geology. 2001;29(11):995–8.

[10] Li C, Jin C, Planavsky NJ, Algeo TJ, Cheng M, Yang X, et al. Coupled oceanic oxygenation and metazoan diversification during the early–middle Cambrian? Geology. 2017;45(8):743–6.

[11] Fan H, Wen H, Zhu X. Marine redox conditions in the early Cambrian ocean: insights from the Lower Cambrian phosphorite deposits, South China. J Earth Sci. 2016;27(2):282–96.

[12] Feng L, Li C, Huang J, Chang H, Chu X. A sulfate control on marine middepth euxinia on the early Cambrian (ca. 529–521 Ma) Yangtze platform, South China. Precambrian Res. 2014;246:123–33.

[13] Zhang ZP. A review on active tectonics and deep crustal processes of the Western Sichuan region, eastern margin of the Tibetan Plateau. Tectonophysics. 2013;584:7–22.

[14] Ma WX, Liu SG, Huang WM, Zeng XL, Zhang CJ, Wang J. Mud shale reservoirs characteristics of Qiongzhusi Formation on the margin of Sichuan basin, China. J Chengdu Univ Technol (Sci & Technol Ed). 2012;39(2):182–9. (In Chinese with English abstract).

[15] Zhang KJ. North and South China collision along the eastern and southern North China margins. Tectonophysics. 1997;270:145–56.

[16] Zhang KJ. Escape hypothesis for the North and South China collision and the tectonic evolution of the Qinling orogen, eastern Asia. Eclogae Geologicae Helvetiae. 2002;95:237–47.

[17] Zhang KJ. A Mediterranean–style model for early Neoproterozoic amalgamation of South China. J Geodynamics. 2017;105:1–10.

[18] Yang JH, Jiang SY, Ling HF, Feng HZ, Chen YQ, Chen JH. Paleoceanographic significance of redox–sensitive metals of black shales in the basal Lower Cambrian Niutitang Formation in Guizhou Province, South China. Prog Nat Sci. 2006;14:52–157.

[19] Geological Survey Academy of Sichuan. 1:2,00,000 Scale Mabian Regional Geological Survey Report. China; 1972. (in Chinese).

[20] Lu FF, Tan XC, Ma T, Li L, Zhao AW, Su CP, et al. The sedimentary facies characteristics and lithofacies palaeogeography during Middle–Late Cambrian, Sichuan basin and adjacent area. Petroleum. 2017;3:212–31.

[21] Liu H, Wang C, Deng B, Deng JH, Xu YL, Zhou W. Geochemical characteristics and Thermal Evolution of Paleogene Source Rocks in Lunpola basin, Tibet Plateau. Pet Sci Technol. 2019;37(8):950–61.

[22] Canfield DE, Poulton SW, Narbonne GM. Late–Neoproterozoic deep–ocean oxygenation and the rise of animal life. Science. 2007;315(5808):92–5.

[23] Cheng M, Li C, Zhou L, Feng L, Algeo TJ, Zhang F, et al. Transient deep–water oxygenation in the early Cambrian Nanhua basin, South China. Geochim Cosmochim Acta. 2017;210:42–58.

[24] Gao P, Liu G, Jia C, Young A, Wang Z, Wang T, et al. Redox variations and organic matter accumulation on the Yangtze carbonate platform during late Ediacaran–early Cambrian: constraints from petrology and geochemistry. Palaeogeogr Palaeoclimatol Palaeoecol. 2016;450:91–110.

[25] Och LM, Shields–Zhou GA, Poulton SW, Manning C, Thirlwall MF, Li D, et al. Redox changes in early Cambrian black shales at Xiaotan section, Yunnan Province, South China. Precambrian Res. 2013;225:166–89.

[26] Zou CN, Wei GQ, Xu CC, Du JH, Xie ZY, Wang ZC, et al. Geochemistry of the Sinian–Cambrian gas system in the Sichuan basin, China. Org Geochem. 2014;74:13–21.

[27] Chang C, Hu W, Fu Q, Cao J, Wang X, Yao S. Characterization of trace elements and carbon isotopes across the Ediacaran–Cambrian boundary in Anhui Province, South China: implications for stratigraphy and paleoenvironment reconstruction. J Asian Earth Sci. 2016;125:58–70.

[28] Pi D, Liu C, Shields–Zhou GA, Jiang SY. Trace and rare earth element geochemistry of black shale and kerogen in the early Cambrian Niutitang Formation in Guizhou province, South China: constraints for redox environments and origin of metal enrichments. Precambrian Res. 2013;225:218–29.

[29] Xu L, Lehmann B, Mao J, Nägler TF, Neubert N, Böttcher ME, et al. Mo isotope and trace element patterns of lower Cambrian black shales in South China: multi–proxy

constraints on the paleoenvironment. Chem Geol. 2012;318:45–59.
[30] Zhou C, Jiang SY. Palaeoceanographic redox environments for the lower Cambrian Hetang Formation in South China: evidence from pyrite framboids, redox sensitive trace elements, and sponge biota occurrence. Palaeogeogr Palaeoclimatol Palaeoecol. 2009;271(3–4):279–86.
[31] Wang X, Shi X, Zhao X, Tang D. Increase of seawater Mo inventory and ocean oxygenation during the early Cambrian. Palaeogeogr Palaeoclimatol Palaeoecol. 2015;440:621–31.
[32] Liu Y, Liu HC, Li XH. Simultaneous precise determination of 40 trace elements in rock samples using ICP–MS. Geochemica. 1996;25:552–8 (In Chinese with English abstract).
[33] Zhang KJ, Li QH, Yan LL, Zeng L, Lu L, Zhang YX, et al. Geochemistry of limestones deposited in various plate tectonic settings. Earth–Science Rev. 2017;167:27–46.
[34] Jones B, Manning AC. Comparison of geochemical indices used for the interpretation of palaeoredox conditions in ancient mudstones. Chem Geol. 1994;111(2):111–29.
[35] Mukul RB. Rare earth element geochemistry of Australian Paleozoic graywackes and mudrocks: provenance and tectonic control. Sediment Geol. 1985;45:97–113.
[36] Mukul RB, Keith AWC. Trace element characteristics of graywackes and tectonic setting discrimination of sedimentary basins. Contrib Miner Petrology. 1986;92:181–93.
[37] Bhatia MR, Crook KAW. Trace element characteristics of graywacks and tectonic setting discrimination of sedimentary basin. Contributions Mineralogy Petrology. 1986;92(2):181–93.
[38] Taylor SR, Mc Lennan SM. The continental crust: its composition and evolition. Oxford: Blachwell; 1985. p. 312.
[39] Zhang KJ, Xia BD, Wang GM, Li YT, Ye HF. Early cretaceous stratigraphy, depositional environment, sandstone provenance, and tectonic setting of central Tibet, western China. Geol Soc Am Bull. 2004;116:1202–22.
[40] Zhang KJ, Li B, Wei QG. Geochemistry and Nd isotopes of the Songpan–Ganzi Triassic turbidites, central China: Diversified provenances and tectonic implications. J Geol. 2012;120:68–82.
[41] Zhang KJ, Cai JX, Zhu JX. North China and South China collision: Insights from analogue modeling. J Geodynamics. 2006;42:38–51.
[42] Jewell PW, Stallard RF. Geochemistry and paleoceanographic setting of central Nevada bedded barites. J Geol. 1991;99:151–70.
[43] Zhang KJ, Zhang YX, Xia BD, He YB. Temporal variations of the Mesozoic sandstone composition in the Qiangtang block, northern Tibet (China): Implications for provenance and tectonic setting. J Sediment Res. 2006;76:1035–48.
[44] Cai JX, Zhang KJ. A new model for the Indochina and South China collision during the Late Permian to the Middle Triassic. Tectonophysics. 2009;467:35–43.
[45] Zhang KJ. Secular geochemical variations of the Lower Cretaceous siliciclastic rocks from central Tibet (China) indicate a tectonic transition from continental collision to back–arc rifting. Earth Planet Sci Lett. 2004;229:73–89.
[46] Arthur MA, Sageman BB. Marine black shales: depositional mechanism and environments of ancient deposites. Annu Rev Earth Planet Sci. 1994;22:499–511.
[47] Deng HW, Qian K. Sedimentary geochemistry and environmental analysis. Lanzhou: Gansu Science and Technology Press; 1993. p. 1–95. (in Chinese).
[48] Jai HC, Yu H. Geochemistry and depositional environment of Mn oxide deposits in the Tokoro belt, Northeastern Hokkaido, Japan. Econ Geol. 1992;87:1265–74.
[49] John RT. Deposition of submarine crusts rich in manganese and iron. Geol Soc Am Bull. 1980;91:44–54.
[50] Yan Z, Wang ZQ, Yan QR, Wang T, Guo XQ. Geochemical constraints on the provenance and depositional setting of the devonian liuling group, east qinling mountains, central china: implications for the tectonic evolution of the qinling orogenic belt. J Sediment Res. 2012;82:9–20.
[51] Rangin C, Steinberg M, Bonnot–Courtois C. Geochemistry of the Mesozoic bedded chert of Central Baja California (Vizcano–Cedros–San Benito): implications for Paleogeographic reconstruction of an old oceanic basin. Earth Planet Sci Lett. 1981;54:313–22.
[52] MuKul RB, Keith AWC. Characteristics of Trace elements in mixed Sandstones and Identification of tectonic Environment in Sedimentary basins. Paleobiology. 1985;11:53–64.
[53] Roser B, Korsch R. Provenance signatures of sandstone–mudstone suites determined using discriminant function analysis of major–element data. Chem Geol. 1988;67(1–2):119–39.
[54] Bischoff JL, Rosenbauer JR. Recent metalliferous sediments in the North Pacific Manganese Nodule Area. Earth Planet Sci Lett. 1976;33:379–88.
[55] Dymond J, Corliss JB, Stillinger R. Chemical composition and metal accumulation rates of metalliferous sediments from site 319, 320, 321. Glasgow: Init. Rep. D. S. D. P. XXXW; 1976. p. 575–88.
[56] Toth JR. Deposition of submarine crusts rich in manganese and iron. Geologieal Soc Am Bull. 1980;9:44–54.
[57] Peter JM, Scott S. Mineralogy, composition, and fluid–inclusion microthermometry of seafloor hydrothermal deposits in the southern trough of Guaymas basin, Gulf of California. Can Mineralogist. 1988;26:567–87.
[58] Smith PA, Cronan DS. The geochemistry of metalliferous sediments and waters associated with shallow submarine hydrothermal activity (Santorini, Aegean Sea). Chemieal. Geology. 1983;39:241–62.
[59] Adriano M, Florian S, Henrik HS, Christian H, Soffian H. The geochemistry and origin of the hydrothermal water erupted at Lusi, Indonesia. Mar Pet Geol. 2018;90:52–66.
[60] Michael MH. Geochemical classification of terrigenouss sand and shales from core or log data. J Sediment petrology. 1988;58(5):820–9.
[61] Marchig V. Brown clays from Central Pacific–Metalliferous sediments or not? Geol Jahrb. 1978;30:3–25.
[62] Steiner M, Wallis E, Erdtmann BD. Submarine–hydrothermal exhalative ore layers in black shales from South China and associated fossils–insights into a Lower Cambrian facies and bio–evolution. Paleogeography. 2001;169:165–91.
[63] Zhai MG. Precambrian Geology of China. New York: Springer Geology; 2015. p. 1–389.
[64] McLennan SM, Hemming S, McDaniel DK, Hanson GN. Geochemical approaches to sedimentation, provenance, and tectonics. Geol Soc Am Spec Pap. 1993;284:21–40.

[65] Floyd PA, Winchester JA, Park RG. Geochemistry and tectonic setting of Lewisian classic metasediments from the early Proterozoic lock marie group of Gairlock, Scotland. Precambrian Res. 1989;45:203–14.
[66] Wedepohl KH. The composition of the continental crust. Geochimica Cosmochimica Acta. 1995;59(7):1217–32.
[67] Mukul RB. Plate tectonics and geochemical composition of sandstones. J Geol. 1983;91(6):611–27.
[68] Chen DQ, Chen G. Applied rare earth element geochemistry. Beijing: Metallurgical Industry Press; 1990. p. 1–268 (in Chinese).
[69] Guo Q, Deng Y, Hippler D, Franz G, Zhang J. REE and trace element patterns from organic–rich rocks of the Ediacaran–Cambrian transitional interval. Gondwana Res. 2016;36:94–106.
[70] Wang C, Liu H, Feng HB, Deng JH, Liu XF, Zhao FF. Geochemistry and U–Pb ages of the diabases from the Luoji area, western Yunnan, China: implications for the timing of the initial rifting of the Ganzi–Litang Ocean. Geologia Croatica. 2019;72:19–32.
[71] Li ZC, Fang X, Liu WG. La–Ce method and Ce isotope geochemistry. Wuhan: Press of China University of Geosciences; 2002. p. 2–56 (in Chinese).
[72] Kunzendorf H, Stoffers P, Gwozdz R. Regional variations of REE patterns in sediments from active plate boundaries. Mar Geol. 1988;84:191–9.
[73] Allegre CJ, Minster JF. Quantitative models of trace element behavior in magmatic processes. Earth Planet Sci Lett. 1978;37:1–25.
[74] Nesbitt HW, Young GM. Prediction ofsome weathering trends of plutonic and volcanic rocks based on hermodynamic and kinetic considerations. Geochimica Cosmochimica Acta. 1984;48:1523–34.
[75] Chen X, Ling HF, Vance D, Shields–Zhou GA, Zhu M, Poulton SW, et al. Rise to modern levels of ocean oxygenation coincided with the Cambrian radiation of animals. Nat Commun. 2015;6:7142.
[76] Akinlua A, Olise FS, Akomolafe AO, McCrindle RI. Rare earth element geochemistry of petroleum source rocks from northwestern Niger Delta. Mar Pet Geol. 2016;77:409–17.
[77] Fan R, Deng SW, Zhang XL. Significant carbon isotope excursions in the Cambrian and their implications for global correlations. Science China–Earth. Science. 2011;41(12):1829–39 (in Chinese).
[78] Xu XB, Lia QM, Gui L, Zhang XF. Detrital zircon U–Pb geochronology and geochemistry of early Neoproterozoic sedimentary rocks from the Northwestern Zhejiang basin, South China. Mar Pet Geol. 2018;98:607–21.
[79] Calvert SE, Pedersen TF. Geochemistry of Recent oxic and anoxic marine sediments: Implications for the geological record. Mar Geol. 1993;113:67–88.
[80] Tribovillard N, Desprairies A, Lallie–Vergès E, Moureau N, Ramdani A, Ramanampisoa L. Geochemical study of organic-rich cycles from the Kimmeridge Clay Formation of Yorkshire (G.B.): Productivity vs anoxia. Palaeogeogr Palaeoclimatol Palaeoecol. 1994;108:165–81.
[81] Bryn J, David ACM. Comparison of geochemical indices used for the interpretation of palaeoredox conditions in ancient mudstones. Chem Geol. 1994;111:111–29.
[82] Anderson RF, Fleisher MQ, Lehuray AP. Concentration, oxidation state, and particulate flux of uranium in the Black Sea. Geoehim Cosmoehim Acta. 1989;53:2215–24.
[83] Morford JL, Emerson S. The geochemistry of redox sensitive metals in sediments. Geochim CosmochimActa. 1999;63:1735–50.
[84] Raymond MC, James BM, Richard IG, Michael DG, Jeffrey RD. Gold and platinum in shales with evidence against extraterrestrial sources of metals. Chem Geol. 1992;99:101–14.
[85] Hatch JR, Leventhal JS. Relationship between inferred redox potential of the depositional environment and geochemistry of the Upper Pennsylvanian (Missourian) Stark Shale Member of the Dennis Limestone, Wabaunsee County, Kansas, U.S.A. Chem Geol. 1992;99:65–82.
[86] Riquier L, Tribovillard N, Averbuch O, Devleeschouwer X, Riboulleau A. The Late Frasnian Kellwasser horizons of the Harz Mountains (Germany): two oxygen deficient periods resulting from contrasting mechanisms. Chem Geol. 2006;233(1–2):137–55.
[87] Nesbitt HW, Young GM. Formation and diagenesis of weathering profiles. J Geol. 1989;97:129–47.
[88] Philipp B, Hans–jürgen B, Michael EB, Bernhard S, Cornelia K, Jens K, et al. Geochemistry of Peruvian near–surface sediments. Geochimica Cosmochimica Acta. 2004;68(21):4429–51.
[89] Sugisaki R, Yamamoto K, Adachi M. Triassic bedded cherts in central Japan are not pelagic. Nature. 1982;298:644–7.
[90] Fedo CM, Nesbitt HW, Young GM. Unraveling the effects of potassium metasomatism in sedimentary rocks and paleosols, with implications for paleoweathering conditions and provenanc. Geology. 1995;23:921–4.
[91] Nesbitt HW, Young GM. Eatly Proterozoic climates and plate motions inferred from major element chemistry of lutites. Nature. 1982;299:715–7.
[92] Liu H, Wang C, Deng JH, Deng B, Li Y, Xu YL. Evaluation of sedimentary features and biomarkers in the Paleogene Niubao Formation in the Lunpola basin, Tibetan plateau: implications for the oil source rocks and exploration. Int J Earth Sci. 2020. doi: 10.1007/s00531-020-01958-x.
[93] Li YD. Study and Evaluation of Shale Reservoir Characteristics of Lower Paleozoic Longmaxi Formation and Qiongzhusi Formation in Changning Region. Southwest Petroleum University; 2014. p. 23–29. (In Chinese with English abstract).
[94] Murray RW. Rare earth elements as indicators of different marine depositional environment in chert and shale. Geology. 1990;18:268–71.
[95] Banerjee DM, Prosun B. Petrology and geochemistry of greywackes from the Aravalli Supergroup, Rajasthan, India and the tectonic evolution of a Proterozoic sedimentary basin. Premmbrinn Res. 1994;67:11–35.
[96] Roser BP, Korsch RJ. Determination of tectonic setting of sandstone–mudstone suites using SiO_2 content and K_2O/Na_2O ratio. J Geol. 1986;94(5):635–50.
[97] Bhatia MR, Taylor SR. Trace–element geochemistry and sedimentary provinces: A study from the Tasman Geosyncline, Australia. Chem Geol. 1981;33(1/2):115–25.
[98] Zhang KJ. North and South China collision along the eastern and southern North China margins. Tectonophysics. 1997;270:145–56.

[99] Zhang KJ, Zhang YX, Li B, Zhong LF. Nd isotopes of siliciclastic rocks from Tibet, western China: Constraints on the pre–Cenozoic tectonic evolution. Earth Planet Sci Lett. 2007;256:604–16.
[100] Zhang KJ, Zhang YX, Li B, Zhu YT, Wei RZ. The blueschist–bearing Qiangtang metamorphic belt (northern Tibet, China) as an in situ suture zone: Evidence from geochemical comparison with the Jinsa suture. Geology. 2006;34:493–6.
[101] Wang C, Liu H, Deng JH, Liu XF, Zhao FF, Wang C, et al. Isotope Geochronologic and Geochemical Constraints on the Magmatic Associations of the Collisional Orogenic Zone in the West Kunlun Orogen, China. Acta Geologica Sin (Engl Ed). 2018;92(2):482–98.
[102] Zhang KJ, Li B, Wei QG, Cai JX, Zhang YX. Proximal provenance of the western Songpan–Ganzi turbidite complex (Late Triassic, Eastern Tibetan Plateau): implications for the tectonic amalgamations of China. Sediment Geol. 2008;208:36–44.
[103] Zhang KJ, Cai JX. NE–trending Hepu–Hetai dextral shear zone in southern China: Penetration of the Yunkai Promontory of South China into Indochina. J Struct Geol. 2009;31:737–48.